Lab on a Chip

CRITICAL REVIEW

View Article Online
View Journal | View Issue

Cite this: *Lab Chip*, 2024, **24**, 1367

Revolutionizing targeting precision: microfluidics-enabled smart microcapsules for tailored delivery and controlled release

Lingling Ren, Shuang Liu, Junjie Zhong * and Liyuan Zhang *

Received 3rd October 2023,
Accepted 9th January 2024

DOI: 10.1039/d3lc00835e

rsc.li/loc

As promising delivery systems, smart microcapsules have garnered significant attention owing to their targeted delivery loaded with diverse active materials. By precisely manipulating fluids on the micrometer scale, microfluidic has emerged as a powerful tool for tailoring delivery systems based on potential applications. The desirable characteristics of smart microcapsules are associated with encapsulation capacity, targeted delivery capability, and controlled release of encapsulants. In this review, we briefly describe the principles of droplet-based microfluidics for smart microcapsules. Subsequently, we summarize smart microcapsules as delivery systems for efficient encapsulation and focus on target delivery patterns, including passive targets, active targets, and microfluidics-assisted targets. Additionally, based on release mechanisms, we review controlled release modes adjusted by smart membranes and on/off gates. Finally, we discuss existing challenges and potential implications associated with smart microcapsules.

1. Introduction

A microcapsule is an inner core droplet that is usually surrounded by an outer polymeric shell. The inner core provides desired space and entraps diverse active materials, while the shell acts as an effective barrier that separates the core from ambient environments.[1] Droplet-based microfluidics is the most effective technology for fabricating microcapsules owing to its precise manipulation of fluids on a low-energy-demand micrometer scale.[2–4] Under the balanced forces between immiscible fluid phases, emulsion droplets are produced and subsequently converted into microcapsules by solidifying the shell.[5,6] However, practical conditions are complex and variable, wherein traditional microcapsules may not always be suitable for their intended applications, particularly when the co-encapsulation of multiple active materials and point-in-time release are required.[7,8] To address these challenges, it is crucial to fabricate smart microcapsules that can achieve the controlled release of encapsulants at specific and pre-designed sites. The biggest advantage of microfluidics-assisted smart microcapsules is that their membranes can be customized to meet specific needs for diverse applications. Smart microcapsules have become promising candidates for controllably encapsulating, transporting, and releasing various active materials in versatile applications, including agricultural,[9,10] food,[11,12] energy,[13,14] biomedical[15,16] cosmetic,[17,18] and chemical industries.[19,20]

Desirable characteristics in smart microcapsules as promising delivery systems are associated with encapsulation capacity, retention, targeted delivery capability, and the controlled release of active encapsulants.[21] Microfluidics-assembled smart microcapsules with engineering structures have been widely explored, such as core–shell microcapsules protecting encapsulants from degradation,[22,23] multiple separate compartments enabling co-encapsulation and drug synergy,[24,25] and responsive membranes achieving stimulus-triggered release to target sites.[26–28] Although there are excellent reviews published on smart microcapsules, some highlight a particular class, such as stimulus-responsive property,[29] smart membranes,[30] or smart gating,[31] and others focus on specific applications.[9,15] In the preparation of smart microcapsules, an important step is not only the selection of an encapsulation carrier for an encapsulant based on final applications, but also the target delivery and controlled release performance, including sites and modes of release. However, reported papers mainly focus on microcapsules transported under specific conditions and then stimulated under external conditions, which is known as passive target. It is of great significance to summarize the most recent advances in microfluidics-assisted smart microcapsules using active target modes as delivery systems in a controlled release manner.

The main focus of this review is to summarize a droplet-based microfluidics emulsion templated smart microcapsule

School of Petroleum Engineering, China University of Petroleum (East China), Qingdao, Shandong, China. E-mail: zhongjunjie@upc.edu.cn, 20210085@upc.edu.cn

in terms of fabrication, target delivery and controlled release. The "smart" of "smart microcapsule" encompasses two essentials: specific target and controlled release. We begin by briefly introducing droplet formation, the selection of suitable microfluidics materials and flexible devices, and the advantages of droplet-based microfluidics. We introduce smart microcapsules as delivery systems, including single-, double-, and high-order emulsion templates and target delivery patterns, including passive and active targets. In addition, the release mechanisms are used as the starting point to present the controlled release procedures adjusted by the smart whole membrane and smart on/off gates. Finally, we discuss the existing challenges and outlooks associated with smart microcapsules.

2. Droplet-based microfluidics for emulsion-templated smart microcapsules

2.1 Mechanisms for emulsion-droplet formation

When two mutually immiscible fluids are introduced into the microfluidics channel, emulsion droplets are produced because of fluid instabilities.[32–34] This phenomenon can be explained by Rayleigh–Plateau instability, where surface tension forces seek to minimize the interfacial area, causing the introduced fluid to become unstable and to form droplets when the surface instability is large enough.[35] The process of droplet formation is a result of a well-controlled balance between various forces acting on the fluid flow in the microscale space, characterized by inertial force, viscous force, gravity, and interfacial tension according to the continuity equation.[36–38] Dimensionless numbers are powerful tools for comparing the relative predominance of various forces and obtaining the necessary fundamental relations in different flow regimes. For example, the occurrence conditions for the dripping regime are $10^{-2} < Ca < 1$ and $We < 1$, while that of the jetting regime is $Ca + We \geq 1$.[32] Table 1 shows the commonly used dimensionless numbers in microfluidics droplet generation, and more detailed information about dimensionless numbers and droplet formation can be found in other reports.[4,39]

2.2 Microfluidics devices for emulsion-droplet formation

2.2.1 Materials for microfluidics devices. Multiple materials can be used to fabricate microfluidics devices, such as glass and polydimethylsiloxane (PDMS) for capillary microfluidics devices,[39,40] polytetrafluoroethylene (PTFE) for fluoropolymer-based microfluidics devices,[41] gelatin methacrylate for 3D printing devices,[15] and polycarbonate for hot-embossing-based microfluidics devices.[42] These materials have been explored to fulfil specific requirements for microcapsule formation. However, different materials for microfluidics device fabrication have advantages and disadvantages. For example, PTFE tubes are not resistant to high pressure, and their upper-temperature limit is around 200 °C. The 3D printing technology is limited by its low resolution, suitable materials, and immature methods for modifying surface wetting properties.[43–47] For droplet-based microfluidics, the most widely used materials are PDMS and glass owing to their processability, flexibility, and low cost.[48] Therefore, we compare the properties and surface modification techniques of glass and PDMS, as summarized in Table 2. The choice of materials for droplet formation depends on the final applications. Glass is a better choice for experiments including organic solvents, such as alkylamines, triethylamine, pentane, and xylenes,[49] because glass devices resist swelling in organic solvents and maintain their geometry under high flow rates and pressure. Moreover, glass devices are suitable for proteins, hydrophobic molecules, or quantifying low concentrations of analytes owing to the low adsorption of the glass. To generate complex emulsions, glass capillary devices are preferred owing to challenges in patterning wettability and local surface modification of PDMS devices.[48] Compared with glass devices, PDMS shows superiority in penalization and small-size droplet production. Considering the high-throughput production of microcapsules, PDMS has greater potential because of its flexibility, which can be designed with parallel devices or multi-layer devices. The surface wettability of droplet-based microfluidics plays an important role in droplet formation, especially PDMS.[46,50] Researchers have made great efforts for surface modification to fabricate complex and smart emulsions (Table 2).

2.2.2 Geometries for microfluidics devices. The basic shear-induced configurations for passive droplet generation are co-flow, flow-focusing, and cross-flow,[61] as shown in

Table 1 Commonly used dimensionless numbers in microfluidics droplet generation

Dimensionless numbers	Symbol	Formation	Physical meaning	Microfluidics value
Reynolds number	Re	$Re = \frac{\rho d u}{\eta}$	Ratio of inertia force to viscous force	10^{-6} – 10
Capillary number	Ca	$Ca = \frac{\eta u}{\sigma}$	Ratio of viscous force to interfacial tension	10^{-3} – 10
Weber number	We	$We = \frac{\rho u^2 d}{\sigma}$	Ratio of inertia force to interfacial tension	<1
Bond number	Bo	$Bo = \frac{\Delta\rho g d^2}{\sigma}$	Ratio of gravity to interfacial tension	$\ll 1$

Table 2 Advantages and disadvantages of different materials and typical surface modification techniques of generators for emulsion droplets

Materials	Advantages	Disadvantages	Emulsion structures	Surface modification techniques	Technique characteristics	Ref.
PDMS	Gas permeability, transparency, biocompatibility, flexibility, easy molding, reproducibility	The poor mechanical property, low surface free energy; instability, deformability	W/O/W, O/W/O	Plasma treatment	A simple and versatile method but the short duration of hydrophilic	51 and 52
			W/O/W	Plasma treatment + coating polyvinyl alcohol (PVA)	Improved plasma treatment and the contact angle was 21.0 ± 3.2° for 30 days	53
			W/O, W/O/W	Adding the surfactant Silwet L-77, Pluronic F-127	Easy to use and the contact angles of the water droplets can be controlled at 52–85° for 10–30 days	34 and 54
			O/W, W/O/W	Sequential layer-by-layer deposition of polyelectrolytes	Allow generating emulsions even after several months	39
			W/O	Coating with a glass-like layer using sol–gel chemistry	Better precision control and chemical robustness, easy to carry out but suffer from poor durability	55
			W/O/W, O/W/O	Covalent with silane + grafting acrylic acid	Spatially modulates the wettability and high contrast spatial patterning	56
Glass	High rigidity, high chemical stability, high strength, impermeability, transparency, easy surface modification, ensure true 3D flow	Limited geometries, limited emulsion size	W/O	Coating PMMA film and silane + laser-induced backside wet etching	Hybrid structures; the ridge is hydrophilic, and the inner surface is hydrophobic	57
			W/O/W, O/W/O	Coating octadecyltrichlorosilane + local UV irradiation for hydrophilization	Locally controlling; forming multiple emulsion droplets	58 and 59
			W/O/W, O/W/O	Coating *n*-octadecyltrimethoxysilane and 2-[methoxy(polyethyleneoxy)6-9--propyl]tris(dimethylamino)silane	Hybrid property of the hydrophilic and hydrophobic surfaces	60

Oil (O), water (W), oil-in-water (O/W), water-in-oil (W/O), oil-in-water-in-oil (O/W/O), water-in-oil-in-water (W/O/W).

Fig. 1. Each of the mentioned basic geometries has its advantages and limitations when used in manufacturing microfluidics devices. The biggest advantage of co-flow geometry is that droplets are formed in a 3D environment, and the surface wettability of channels can be neglected.[32] The flow-focusing devices can generate extremely small-size droplets (<10 μm) and maintain a moderate coefficient of variation (CV).[61,62] The cross-flow devices can produce better size-controlled monodisperse droplets, with a CV of less than 2%[32] and are widely used to fabricate parallel microfluidics devices for mass production. A comparison of droplet generators is provided in Table 3.

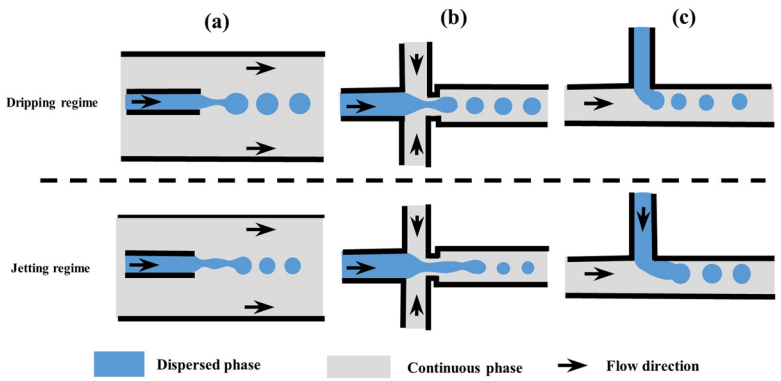

Fig. 1 Schematic of microfluidic droplet generators with dripping and jetting regimes (not to scale). (a) Co-flow, (b) flow-focusing, and (c) T-junction. Modified with permission from ref. 63. Copyright 2013, IOP Publishing Ltd. Printed in the UK and USA.

Table 3 Critical parameters of different droplet generators

Geometries	Emulsion structures	Mean size (μm)	Coefficient of variation	Ref.
Cross-flow	W/O	90–120	<5%	36
	O/W, W/O	131.5	1.35%	74
	O/W	96.4	1.3%	75
Co-flow	O/W/O	156	3.88%	76
	W/O	210	1.20%	77
	O/W/O	270	1.38%	78
	O/W	2–200	<3%	79
Flow-focusing	O/W/O	198.2	2.4%	80
	O/W	10–50	3.9%	81
	W/O	153	5%	82
One-step	O/W/O/W	92	2%	83
	O/W/O	181	1.5%	84
	W/O/W	160	1.6%	85
	O/W	107	3.1%	86
	W/O/W/O	181	2%	87

Freely combined with the three shear-induced geometries, multi-step, one-step, and high-throughput microfluidics devices were designed for innovative droplet generation, as shown in Fig. 2. Generally, a multi-step microfluidics device is used to connect multiple basic geometries with opposite wettability in series, such as two consecutive cross-flow devices,[64] two flow-focusing devices,[65] and four co-flow devices.[66] However, it is difficult for the multi-step device to precisely control spatial wettability; thus, full control over the relative sizes of the core and the shell of the emulsions is challenging. A one-step microfluidics device can be fabricated by simultaneously converging three phases into one point and providing high precision for aggregate formation. For example, a facial one-step microfluidics device was designed for the quick production of smart microcapsules with controllability and scalability, enhancing the ability to control the process of emulsion generation.[67,68] However, a good alignment of the tubes is necessary on a micron scale, which is a labor-intensive process. To resolve this problem, a novel design without manual adjustment for coaxial alignment was fabricated by simply inserting an annular capillary array into a collection channel, which maintained a fixed coaxial alignment and allowed the innermost flow to be sheathed by the middle phase.[69] Moreover, the high-throughput generation of microcapsules has been achieved using parallelized microfluidics flow-focusing devices.[70] A reported parallelized device for mass production was multiple parallel droplet generators coupled to only two inlets and achieved a throughput of 8.2 L h^{-1}.[71] Using parallel droplet microfluidic, Headen *et al.* achieved 600% increased throughput for cell encapsulation compared to single-droplet device.[72] Additionally, Shin *et al.* designed a multi-layer drop maker geometry to fulfill the mass production of droplets for the remediation of heavy crude oils.[73]

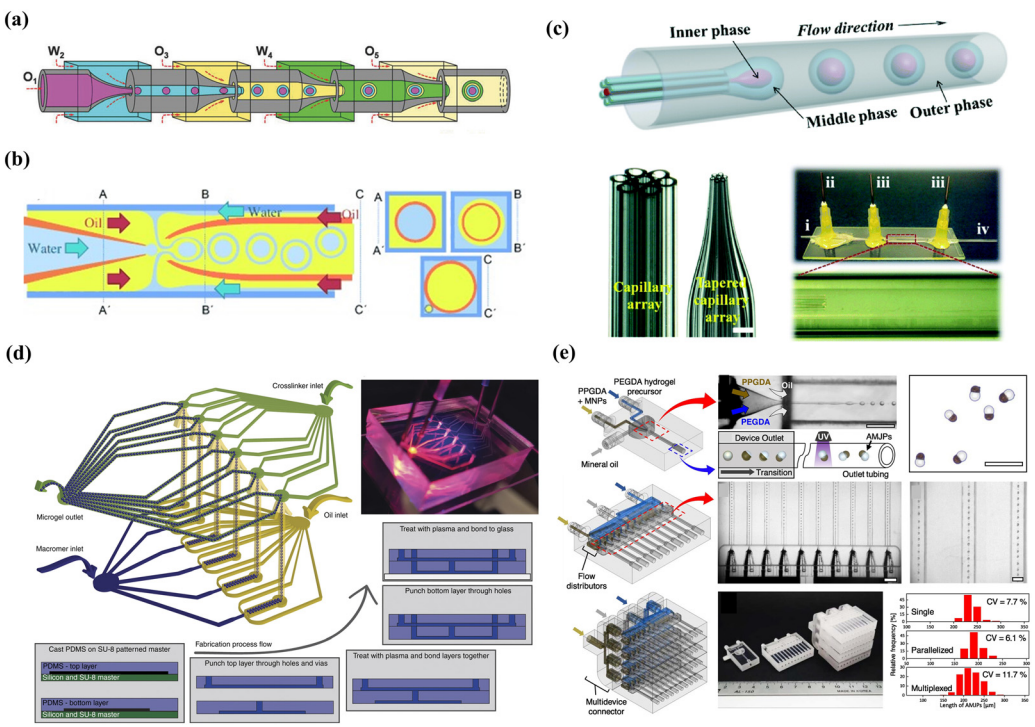

Fig. 2 Combined microfluidics devices: (a) multi-step microfluidics device. Reprinted with permission from ref. 66. Copyright 2018, WILEY-VCH Verlag GmbH & Co. KGaA, Weinheim. (b) One-step microfluidics and the three cross-sectional schematics (A–A', B–B', and C–C') are included for clarity. Reprinted with permission from ref. 88. Copyright 2011 WILEY-VCH Verlag GmbH & Co. KGaA, Weinheim. (c) Advanced one-step microfluidics and the i–iv are the inner, middle, outer and collection channels, respectively. Reprinted with permission from ref. 69. Copyright 2014 Royal Society of Chemistry. (d) Parallel microfluidics device. Reprinted with permission from ref. 72. Copyright 2017, Springer Nature. (e) Multi-layer microfluidics devices. Reprinted with permission from ref. 73. Copyright 2023 Elsevier B.V.

2.3 Advantages of droplet-based microfluidics for smart microcapsules

Compared with traditional emulsification technologies that rely on bulk properties of emulsions and output energy, microfluidics technology offers significant advantages for generating different emulsions with the desired dispersity and size on a low-energy-demand micrometer scale.[4] Through laminar fluidic patterns and dominant convection effects, microfluidics techniques enable precise control of fluid dynamics, contributing to the highly monodisperse and controllable size emulsion droplets. For example, droplets obtained from traditional methods exhibit a CV of 7–15%, while microfluidics droplets achieve much lower values of 1–5%.[89,90] Moreover, different droplet diameters ranging from 5 to 1000 μm can be controlled in microfluidics by precise control of the relative flow rates between the two phases.[91] Reports showed that decreasing the flow rate of the outer phase from 8000 μL h^{-1} to 2000 μL h^{-1} reduces droplet size from 60 μm to 40 μm and maintained droplets with a CV as low as 1.3%.[61,91,92] However, by adjusting the flow rate to control the size of droplets, a problem that needs to be considered is that the ultrahigh flow rate can block and stagnate the channels, causing excessive material consumption and droplet instability.[36]

By precisely manipulating composition and tailorable interfaces between continuous and dispersed phases, microfluidics techniques offer flexibility in achieving shape-controlled microcapsules. Typically, channel geometries are commonly employed to manipulate the shape of emulsion droplets. An example is the helical-shaped microcapsules fabricated using two square capillaries to connect the injection, transition, and transformation tubes under the liquid rope coiling effect.[92] A Y-shaped channel and planar sheath-flow geometry were utilized to produce biphasic Janus droplets.[93] Alternatively, precisely tailoring interfacial tension of multiple interfaces by microfluidics offers a promising approach to fabricating microcapsules with flexible shapes, including Janus,[94] snowman-like[95] and dumbbell-shaped.[96] However, non-spherical-shaped microcapsules are unstable owing to the interfacial minimum free energy effect. To enhance droplet formation stability, an obstacle-assisted microfluidics device was designed by incorporating an obstacle into the outlet channel.[97] In addition, using a polyethylene glycol-modified protein-surfactant to stabilize microcapsules, non-spherical emulsion droplets could be stable against coalescence for months and maintained non-spherical shapes for hours, which offered new opportunities for shape-relevant studies.[98]

The free combination of basic geometries endows the fabrication of microcapsules with more sophisticated structures and morphologies that cannot be achieved by traditional fabrication methods.[99] Owing to the excellent controllability and remarkable scalability of microfluidics, multiple compartments could be designed with specific core numbers, ratios, and sizes, benefiting from the synergistic encapsulation of multiple materials.[100] The greater potential of microfluidics lies in synthetic cells with physiologically relevant environments by applying a high-throughput microfluidics method.[101] Meanwhile, microfluidics systems provide more stable reaction conditions and reduce reagent consumption, thereby efficiently preventing cross-contamination and simplifying post-processing.[102]

3. Smart microcapsules for target delivery

Delivery systems are the prerequisite and key to the success of target delivery. In this chapter, we begin by summarizing emulsion-templated microcapsules as delivery systems, followed by introducing the target delivery patterns, including passive target, active target, and microfluidic-assisted target.

3.1 Emulsion templated microcapsules as delivery systems

An ideal delivery system should encapsulate the encapsulants as efficiently as possible and overcome a series of barriers to easy transport to the target sites. Emulsion-templated microcapsules manufactured through emulsion templating and subsequent solidification are promising candidates for delivery systems owing to their flexible manipulation to functionalize the separated phases and interfaces by physical/chemical processes. The emulsion templates typically include single emulsion, double emulsion, and high-order emulsion. We summarized the emulsion-templated microcapsules as delivery systems to encapsulate different active materials for diverse applications in Table 4.

3.1.1 Single emulsion templated delivery systems for efficient encapsulation. Single emulsion templated micro-vehicles are usually engineered into solid microparticles with homogeneous structures or heterogeneous structures. Single emulsion droplets offer scalability, high rate, and low-cost advantages compared to double emulsions for controllable encapsulation.[118] By the advantage of monodisperse single emulsion droplets, attractive containers with homogeneous structures (Fig. 3(a)) were fabricated through cross-linking poly(ethylene glycol) diacrylate to encapsulate living yeast and bacteria.[119] Solid microparticles with heterogeneous structures could be fabricated by the microfluidics device with a θ-shaped injection tube[120,121] (Fig. 3(b)). However, the consistent frequency of droplet formation is limited to a specific range of flow rates, restricting the adjustment of Janus droplet template morphologies and sizes.[122] Alternatively, combining the microfluidics technique and phase separation provides an opportunity for Janus microparticles. For example, monodisperse amphiphilic Janus microparticles were fabricated by phase separation-induced co-solvent diffusion and dewetting, whose morphologies could be flexibly and precisely controlled by adjusting the flow rates and compositions of different phases.[123,124] It is worth mentioning that the Janus particle

Table 4 Summary of emulsion templated delivery systems for various applications

Structures	Key materials	Emulsification	Encapsulants	Characteristics	Applications	Ref.
O/W	Poly(lactic-*co*-glycolic acid) (PLGA) in dichloromethane/1% PVA	Evaporation of solvent	Bupivacaine	Biodegradable matrix; lower initial burst	Drug delivery	103
W/O	4 wt% biocide, 40 wt% PEGDA, 1 wt% photoinitiator, fluorescein sodium salt/98 wt% dodecane, 2 wt% EM 90	UV polymerization	Grotamar71	Microcapsules maintain their shapes for more than 6 weeks in oil and exhibit antimicrobial activity	Agriculture industry	104
O/W	Soybean oil containing crosslinking agent terephthalaldehyde/chitosan aqueous solution	Interface crosslinking reaction	Tea tree oil	The storage time can be up to 150 days	Personal-care	105
O/W	Methyl methacrylate, isophorone diisocyanate, azobisisobutyronitrile, pentaerythritol tetraacrylate, Span 80/Tween 80, diethylenetriamine	Interfacial polymerization and suspension-like polymerization	*N*-Hexadecane	The encapsulation ratio of 94.5%	Energy storage	106
W/O	20 wt% PEGDA, 10 wt% NaSS, 20 wt% glycerin, photoinitiator 2 wt% Darocur 1173/paraffin oil, 0.5 wt% Abil EM 90	Ultraviolet (UV) polymerization	*Bacillus subtilis*	The encapsulation efficiency of bacterial was almost 100%	Enhanced oil recovery	107
W/O/W	2 w/v%, PVA/dichloromethane, 7 w/v% PLGA, 0.7 w/v% rifampicin, 5 v/v% span 80/2 w/v% PVA	Solvent evaporation	Rifampicin	The drug encapsulation efficiency is 78.5 ± 1.1%	Drug delivery	108
O/W/O	Soybean oil/Pluronic F127, glycerin/soybean oil, poly (*N*-methylolacrylamide)	Free radical polymerization	Sodium dodecyl benzene sulfonate	The efficient encapsulation avoids the adsorption loss of surfactants	Enhanced oil recovery	13
O/W/O	Soybean oil, benzyl benzoate, Sudan III/sodium alginate, calcium-ethylenediaminetetraacetic acid, D-(+)-gluconic acid δ-lactone/soybean oil, 5 w/v% PGPR 90	Solvent diffusion-ionic crosslinking	Citral	Under mild conditions, without high temperature, UV irritation, or acetic acid	Food antioxidant	76
W/W/W	15 wt% dextran, 0.5 wt% poly(diallyldimethyl ammonium chloride)/17 wt% polyethylene glycol/polyethylene glycol, polystyrene sodium sulfate	Electrostatic attraction	Platelet-derived growth factor-BB	Without organic solvents; maintain the biological activities of proteins	Sensitive biomarkers	68
O–W–O	8% w/v PEG (35 kDa), 17% OptiPrep densifier/4–8% w/v 4-arm maleimide,10 mM triethanolamine/-mineral oil, 0.5 v/v% Span-80	Michael addition-mediated gelation	Hepatocyte cells	Encapsulants maintained inside the microcapsules for over ten days	Cell culture	109
W/O/W	Sodium alginate/ethyl cellulose/PVA	Ionic cross-linking and solvent evaporation	Phycocyanin	Encapsulation efficiency of up to 98%	Colon-targeted delivery	110
W/O/W	Diethyl phthalate, diisodecyl phthalate, pentane, cyclopentane, cyclohexane, heptane/37 wt% glycidyl methacrylate, 24 wt% ethylene glycol methacrylate, 4.5 wt% 2-hydroxy-2--methylpropiophenone, 1 w/w% 2--hydroxy-2-methylpropiophenone/2 wt% PVA	UV polymerization	Nile red and fluorescein salt	Strong microcapsules; encapsulating materials in the core and shell	Applications requiring mechanical stability	111
W/O/W	5% PVA and 4% Tween 80/photocurable oil/5% PVA	UV polymerization	α-Pinene	After approximately 2.8 days of dispersion in water, 85 ± 8% of α-pinene remained in microcapsules	Cosmetic industry	112
W/W/O	NIPAm-poor, Span 80/NIPAm-rich, oleophilic, Pluronic F-127, glucose oxidase-loaded silica nanocontainers/silicon oil, 5 v/v% DC749	UV polymerization	Glucose oxidase-loaded silica nanocontainers	The outer shell serves as the gateway for the transport of smaller molecules; controllable enzymatic reactions	Glucose sensors	113
W/O/W	Glycerol/fatty glycerides/glycerol, PVA	Liquid-to-solid phase transition	FITC-dextran	These microcapsules remain stable at room temperature for at least six months, with uniform mechanical properties	Multiple compartments and robust microcapsules are desired	114

Table 4 *(continued)*

Structures	Key materials	Emulsification	Encapsulants	Characteristics	Applications	Ref.
W/O/W	Poly(*n*-vinyl caprolactam), 20 w/w% PVA/ethoxylated trimethylolpropane tri acylate, 1 w/w% photoinitiator/10 w/w% PVA	UV polymerization	Kinetic hydrate inhibitors	Release encapsulant only at temperature responsible for hydrate formation under shear flow	Deepwater oil and gas production	115
W/O/W/O	The aqueous solution containing hydrophilic actives/hexadecane/10% PEGDA, 2% PVA/2% Span 80, mineral oil	UV polymerization	Erioglaucine or fluorescein sodium salt	The hydrophilic cargoes exhibited 3 months of retention	Biomedicine	116
O/W/O/W	α-Pinene/2% PVA/photocurable ethoxylated trimethylolpropane triacrylate/10% PVA	UV polymerization	α-Pinene	The encapsulation efficiency is above 95%	Fragrances application	83
(W/O)/W/O	Nanoparticles/1% w/v Pluronic F127, NIPAM, *N*,*N*′-methylenebisacrylamide, 2,2′-azobis(2-amidinopropane) dihydrochloride/soybean oil, 8 w/v% PGPR 90	UV polymerization	FluoSphereÒ beads	Nanoparticles are encapsulated in microcapsules without any leakage before sites on demand	Pharmaceutical industry	117

has great importance in emulsion stabilization owing to its smart convertible amphiphilic property.[125]

Generally, the commonly used single emulsions include W/O and O/W. The former is suitable for water-soluble cargo, such as Grotamar[104] and the latter works well for hydrophobic cargo, such as curcumin.[86] Using W/O emulsions as the protector to encapsulate cells, cell-laden delivery systems are significant for *in situ* delivery in tissue engineering.[126]

Moreover, W/W emulsions can be used to encapsulate active materials.[127] However, the low interfacial tension in W/W emulsion makes droplet formation difficult and not conducive to encapsulate. To resolve this problem, mechanical shaking was introduced to the device to fabricate stable W/W emulsions, which provide small pulses and facilitate jet break-up.[128] In addition, protein particles[129] and polydopamine particles[130] are used to stabilize W/W emulsions. Interfacial precipitation and interfacial gelation could also be introduced to enhance the encapsulation efficiency of W/W emulsions.[128]

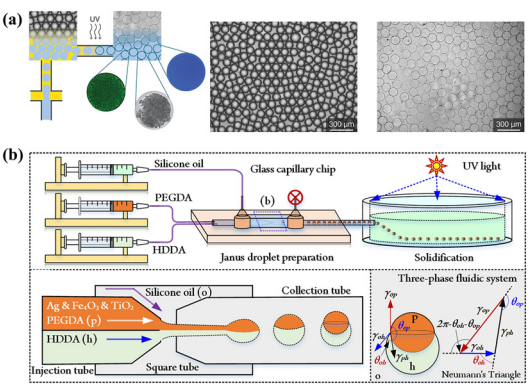

Fig. 3 Single emulsion-templated microparticles with homogeneous structures or heterogeneous structures. (a) Microfluidics device for single emulsion-templated microparticles with a homogeneous structure. Reprinted with permission from ref. 119. Copyright 2023, American Chemical Society. (b) Microfluidics device with a θ-shaped injection tube for single emulsion-templated microparticles with heterogeneous structures. Reprinted with permission from ref. 120. Copyright 2023, Elsevier B.V.

Co-encapsulating hydrophilic and hydrophobic materials in single emulsion templated delivery systems poses a challenge owing to the nature of the emulsion core (hydrophilic or hydrophobic). Incorporating micro/nanoparticles in the matrix offers a promising solution to address this issue and enhances encapsulation efficiency without chemical conjugation. For instance, embedding porous silicon particles into the dispersed oil phase of O/W microcapsules to encapsulate hydrophilic atorvastatin and hydrophobic celecoxib is directly added to the oil phase.[131] Another effective approach involves using halloysite nanotubes embedded in a polymer matrix to achieve the co-encapsulation of drugs with different physicochemical properties.[117]

3.1.2 Double emulsion-templated delivery systems for efficient encapsulation. Double emulsion-templated microcapsules with a core–shell structure allow encapsulating materials inside the core, and the shell acts as a diffusion barrier to enhance retention for efficient encapsulation. Using different shell solidifications, the shell could be engineered into a dense shell, porous shell, colloidal particle shell, and polymersome shell, as shown in Fig. 4.

Microcapsules with dense shells have the properties of low permeability and mechanical and chemical stability, which are suitable for delivery systems that require highly efficient encapsulation, long-term storage/isolation without leakage, and no need for molecular exchange in the delivery process. The polymerization and consolidation of polymers are appropriate methods for dense shell formation. Some active encapsulants with poor chemical stability are commonly encapsulated in delivery systems with dense shells. For example, an encapsulation ratio of 94.5% of the thermal energy storage system was developed to encapsulate

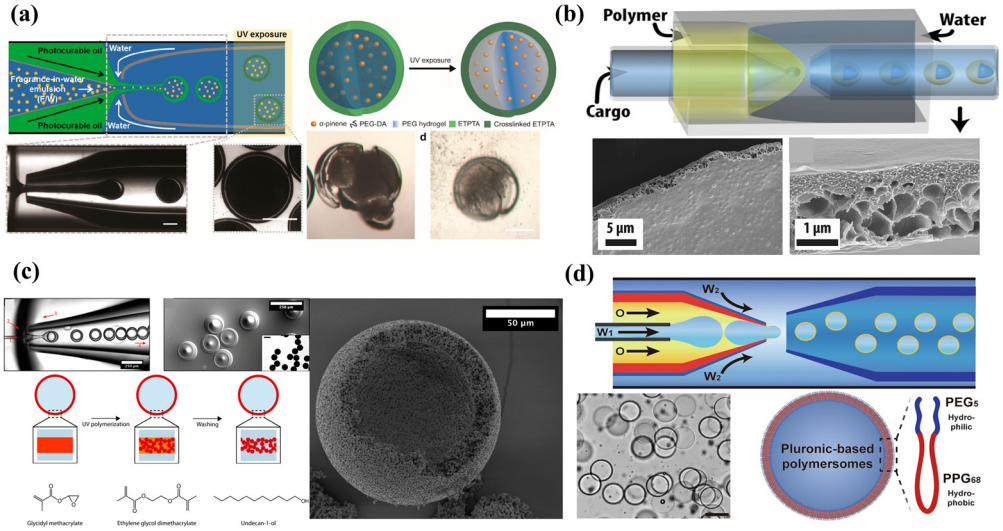

Fig. 4 Microcapsules with different shells: (a) microcapsules with dense shells. Reprinted with permission from ref. 112. Copyright 2016, American Chemical Society. (b) Microcapsules with porous shells. Reprinted with permission from ref. 134. Copyright 2020, American Chemical Society. (c) Microcapsules with colloidal particle shells. Reprinted with permission from ref. 135. Copyright 2017, American Chemical Society. (d) Microcapsules with polymersome shells. Reprinted with permission from ref. 136. Copyright 2022, Springer Nature.

N-hexadecane by hybrid and sense polymer shells of polyurea and poly(methyl methacrylate).[106] Delivery systems with dense shells also play a key role in mitigating volatile materials.[132] A typical example is the fragrance-in-water emulsion-assisted microcapsules, in which a dense shell was fabricated by copolymerizing trimethylolpropane ethoxylate triacrylate and PEGDA and achieving an encapsulation efficiency of α-pinene above 95%.[83] To avoid the adsorption loss of surfactants for enhancing oil recovery, the microcapsule with a dense shell was a promising delivery system for targeting the delivery of surfactant to the residual oil.[13] Delivery systems with dense and stable shells are also necessary to protect the structure and activity of proteins from the negative influence of the gastrointestinal environment. By introducing hydrogen bonds between molecules to construct the stable shell, a high encapsulation efficiency of up to 98% was achieved, and the stability and bioavailability of phycocyanin were improved.[110] The dense shell thickness is an important parameter for mechanical properties and can be adjusted by microfluidics precursor concentration, flow rate, and viscosity. Homogeneous shell thickness is conducive to maintaining mechanical stability but requires higher osmotic pressure for encapsulant release, which may not be suitable for certain biomedical applications. An inhomogeneous dense shell was fabricated by adjusting the flow rate ratio of the middle and inner phases.[133] Under low osmotic pressure conditions, the weakest spot of the inhomogeneous shell swells and eventually ruptures, allowing for encapsulant release.

Semipermeable microcapsules with porous shells are commonly used to selectively encapsulate active materials and ensure the interaction between the internal and the surrounding environment, especially for cell encapsulation. Porous membranes could be fabricated by inner droplets as templates, then creating pores in the shell or directly forming a porous shell.[137,138] The permeability of the porous shell is determined by the porosity and the size of pores, which allow transporting the smaller materials compared to the pore size. For example, using butyl-acetate as a porogen, semi-permeable biocompatible microcapsules with pore diameters below 30 nm were fabricated through polymerization-induced phase separation, which could encapsulate proteins and enzymes larger than 32.7 kDa and allow for the permeation of smaller molecules.[139] Using polyethylene oxide as the porogen, β-cell with high cell viability (>90%) was encapsulated in the delivery system with a porous alginate shell, which protected β cells from immune rejection and allowed the exchange of small molecular nutrients during transplantation.[140] The commonly used porogens are hydrocarbon waxes, carbohydrates, gelatin, and sugars.[141] However, caution must be exercised to remove the porogen to prevent negative effects on morphology.[89] Therefore, permanent geometric templates and self-assembling dendrimer-dye complexes have been introduced to enable the production of monodisperse porous microspheres with well-defined pores.[141] It is difficult for porous delivery systems to combine permeability, selectivity, and mechanical stability. To balance these three features, a phase-inversion technique was introduced to fabricate a strong and permeable porous shell. An example is the asymmetric graded macroporous shell designed by Wu *et al.*, and in their report, the microcapsules unbuckle slowly and recover a spherical shape in high osmotic pressure (PEG-6000, 0.1 mol L^{-1}).[134]

The colloidal particles adsorbed to emulsion templates are connected into a densely packed colloidal particle shell, which could be termed a colloidal microcapsule.[142,143] Delivery systems with colloidal particle shells are preferred for encapsulating active materials that require ultrahigh porosity, a large contact surface area, and internal structural control.[144] Inorganic and organic nanoparticles could be used to form colloidal shells, whose pore size could be studied by monitoring dye molecules with different hydrodynamic diameters.[145,146] The permeability of the colloidal shell can be controlled through the radii of the coating particles and post-fabrication treatment.[147] The pore size between particles is about 10% of the radius of particles.[148] The pore size is usually more than 50 nm by colloidal self-assembly or phase separation of polymers, while the microphase separation of block polymers provides a pore size of 5–50 nm.[149–151] Encapsulants, which are smaller in size, can diffuse through these shells. For instance, a porous shell made of 20 nm shellac nanoparticles crosslinked by telechelic polymers can allow for the transport of 1 nm rhodamine B while encapsulating 60 nm particles in the cores.[152] In particular, when the molecular size is significantly smaller than the pore size, the transport rate of the encapsulants is not affected by the size of the particles that form the shell.[153] To enhance the mechanical property of the colloidal shell, low diluent concentrations and densely interconnected particle networks were designed and exhibited a force at a break up to 200 mN.[135] Instead of self-assembly to form densely packed colloidal particles, electrostatic interactions were introduced to complex the negatively charged shellac nanoparticles and the positively charged telechelic polymer, thus developing a porous ultrathin shell for selective permeability.[152]

Polymersomes (also referred to as polymeric vesicles) are vesicles with membranes composed of bilayers of macromolecular amphiphilic block-copolymers, diblock, triblock, graft, and dendritic copolymers.[154] Polymersomes serve as delivery systems that exhibit high stability, versatility, and the capacity to simultaneously encapsulate hydrophilic and hydrophobic materials.[155] The hydrophilic substances are usually encapsulated in their aqueous lumen while the hydrophobic molecules are encapsulated within their membranes owing to the adjusted chemical composition and thickness of membranes. The thickness of the membrane could be adjusted by tuning the length and composition of the amphiphilic block-co-polymers, ranging from 2 nm to 47 nm.[156] The thicker membranes allow for more efficient entrapment of hydrophobic drugs as well as smaller nanoparticles. For example, hydrophobic gold nanoparticles (9 ± 2 nm) were incorporated within the hydrophobic portion of the shell to achieve laser light trigger release, while nanoparticles above 7 nm could not be encapsulated within the membranes of liposomes.[157] Compared to liposomes, the dilemma of polymersomes is the modulation of stability and permeability.[158] With the precise control of microfluidics, Pluronic L121 polymersomes with stable and semi-permeable properties were fabricated and achieved spatiotemporal control of enzymatic reactions in artificial cell-like, enabling the formation of artificial cell models.[136]

To simultaneously encapsulate different materials in a single vehicle without cross-contamination, multicompartment microcapsules are good candidates for delivery systems. Multicompartment microcapsules can be categorized as concentric multi-compartments (multi-shells)[159] and parallelly multi-compartments (multi-cores).[100]

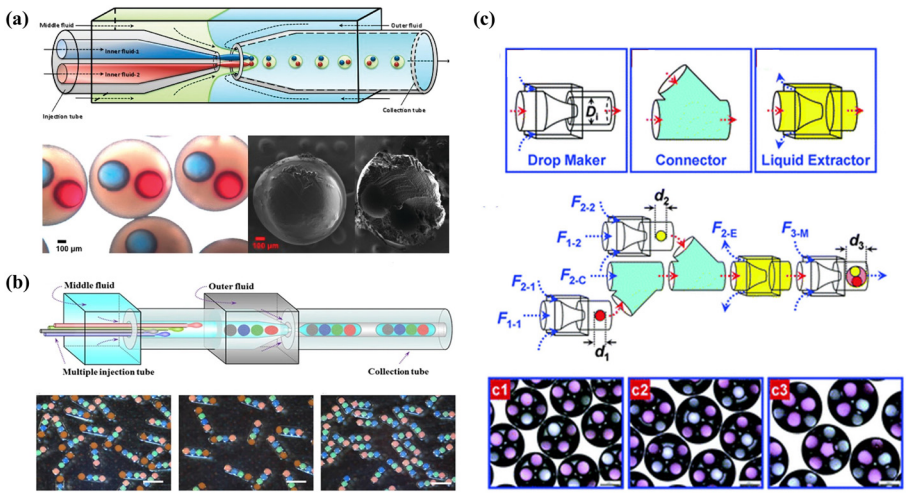

Fig. 5 Double emulsion templated microcapsules with multi-cores fabricated using different microfluidics devices. (a) Microcapsules with two components fabricated using two inner channels in a microfluidics device. Reprinted with permission from ref. 114. Copyright 2010, American Chemical Society. (b) Rod-like microcapsules with position-indexed photonic crystal cores fabricated using multiple inner channels in a microfluidics device. Reprinted with permission from ref. 24. Copyright 2012, Springer Nature. (c) Microcapsules with quadruple-component (c1), quintuple-component (c2), and sextuple-compoment (c3) fabricated using different combinations of building blocks. Reprinted with permission from ref. 7. Copyright 2011, the Royal Society of Chemistry.

For double emulsions, concentric multiple compartments usually refer to the simultaneous encapsulation of the core and shell.[160] Multi-core delivery systems could be fabricated by employing multiple-inner channels in a microfluidics device[24] (Fig. 5(a) and (b)), or by designing hierarchical and scalable microfluidics devices (Fig. 5(c)). By flowing quantum dots in one inner channel and ferric oxide in the other inner channel, multi-core anisotropic magnetic microcapsules were fabricated, which encapsulated quantum dots and ferric-oxide in separate cores.[161] Deng *et al.* utilized independent droplet streams and adjusted interfacial energies to produce multicompartment liposomes.[162] By changing the relevant flow rates of drop maker fluids and thus changing the formation rates and numbers of droplets, microcapsules with controlled array quadruple cores were produced.[100] In addition, five separate internal channels in a microfluidics device were used to produce smart microcapsules with five cores.[24]

3.1.3 High-order emulsion templated delivery systems for efficient encapsulation. With flexible combinations of structures and compositions, high-order emulsion-templated microcapsules as delivery systems enable the efficient encapsulation of active materials, which can be fabricated by one-step or multi-step droplet generators, as shown in Fig. 6. High-order emulsion templated delivery systems enable the diverse and flexible encapsulation of active materials. Using O/W/O/W triple emulsions as templates, a delivery system with an ultrathin water layer was fabricated, achieving a high encapsulation efficiency of 95% and extending the storage time of hydrophobic α-pinene.[83] By fabricating W/O/W/O triple emulsion templates, hydrogel delivery systems, with an intermediate oil layer working as an effective diffusion barrier, encapsulated hydrophilic sodium salt into the aqueous core with a storage time of 3 months.[116] Inspired by natural cells, Chu *et al.* mimicked nonenzymatic antioxidant defense systems and fabricated triple emulsion templated carriers for highly reactive antioxidants, achieving 94.6 ± 4.25% encapsulation efficiency after a month.[163] To ensure a more efficient encapsulation capacity, it is highly demanding to produce carriers with thin shells and maximize core volume. High internal osmosis in W/O/W/O triple-emulsion droplets was used to produce delivery systems with large water cores.[87] The higher innermost osmosis of the water core caused the inward flux of water along with the rupture of the oil layer, thus expanding the core and shrinking the hydrogel shell.

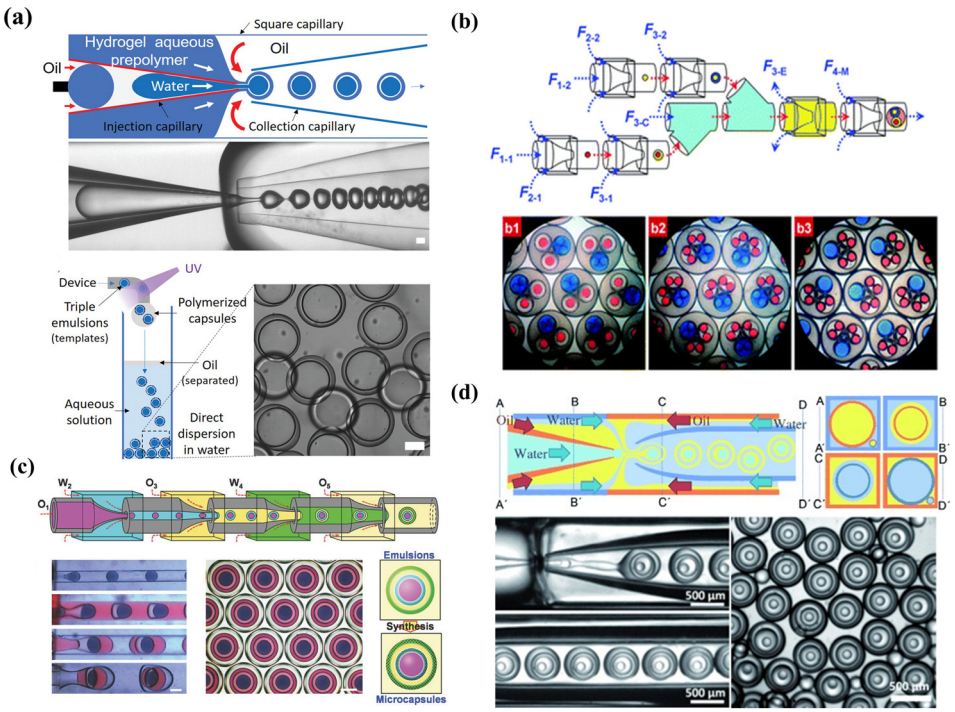

Fig. 6 High-order emulsion-templated microcapsules fabricated using different microfluidics devices. (a) W/O/W/O triple emulsion templated microcapsules fabricated using a one-step microfluidics device. Reprinted with permission from ref. 116. Copyright 2020, Wiley-VCH GmbH. (b) O/W/O/W triple emulsion templated microcapsules fabricated using a multi-step microfluidics device with a combination of three building blocks. b1 and b2 are triple emulsions containing two different double emulsions respectively. b3 is triple emulsions containing one single emulsion and two double emulsions. Reprinted with permission from ref. 7. Copyright 2011, the Royal Society of Chemistry. (c) O/W/O/W/O quadruple emulsion templated Trojan-horse-like microcapsules fabricated using a multi-step microfluidics device. Reprinted with permission from ref. 66. Copyright 2018, WILEY-VCH Verlag GmbH & Co. KGaA. (d) W/O/W/O/W quadruple emulsion templated microcapsules fabricated using a one-step microfluidics device and the four cross-sectional schematics (A–A', B–B', and C–C') are included for clarity. Reprinted with permission from ref. 88 Copyright 2011, WILEY-VCH Verlag GmbH & Co. KGaA, Weinheim.

In addition to triple emulsion templates, quadruple emulsion templated microcapsules, especially concentric multi-compartments, were fabricated for efficient encapsulation. Using W1/O2/W3/O4/W5 quadruple emulsions as templates, Lee *et al.* manufactured multi-shell microcapsules with concentric multi-compartments for encapsulating distinct reagents.[164] To enhance encapsulation efficiency, the W1/O2/W3 double-emulsion drops flow through a core stream of the outer core–sheath flow W3/O4, and the O2 and O4 were fabricated by ultrathin shells. Another novel Trojan-horse-like delivery system with concentric multi-compartments was reported by applying one-step quadruple template synthesis, in which nested inner core and outer compartments could separately encapsulate different materials by incorporating two stimulus-responsive functional shells into their inner and outer aqueous layers.[66]

3.2 Smart microcapsules for target delivery

3.2.1 Passive target delivery. Passive target is the preferential approach for target delivery by which microcapsules deliver their payloads selectively to the target sites, achieving localization and aggregation of carriers. The carrier-based accumulation of passive target could be controlled by the physicochemical properties of carriers and the specific stimuli of target sites.

Physicochemical properties-mediated passive target. Physicochemical property-mediated passive target could be adjusted by size,[165,166] charge,[167] shape,[168] and rigidity[169] of carriers to achieve local accumulation at the target sites. Optimization of these parameters helps to enhance targeting accumulation and maximize delivery efficacy.[167] The primary factor is the carrier size, especially for the enhanced permeability and retention (EPR) effect in drug delivery,[170] which limits the size of drug carriers to 10–200 nm.[171] The size could be tuned by the microfluidics-assisted flow rate, flow ratio, concentration, or molecular weights of the precursors.[166] Carriers of varying sizes exhibit distinct targeting efficiencies, leading to different tissue distribution and localization patterns.[172] For example, the smaller carriers (5–15 nm) were cleared using follicular dendritic cells within 48 hours, while the larger carriers (50–100 nm) could be retained over 5 weeks, resulting in a 175-fold increase in antigen delivery compared to the smaller ones.[173] Carriers exceeding 100 nm in size demonstrate enhanced retention effects within blood vessels but exhibit limited penetration within the dense tumor matrix.[174] The smaller carrier is the opposite. Therefore, delivery systems with a constant particle size face challenges in achieving both efficient "penetration" and prolonged "retention" simultaneously. To achieve efficient target delivery, delivery systems with variable particle sizes are a promising strategy for effective treatment.[175] However, owing to the different targeting conditions, the efficiency of physicochemical property-mediated passive target is not always satisfactory, especially for highly sized heterogeneous human tumors.[176] A meta-analysis reported that only an average of 0.7% of the injectable dose was found to be delivered to the tumor[177] because physicochemical property-based passive target is not only affected by synthetic properties but also by targeting physiological characteristics. Sykes *et al.* studied the influence of tumor volume on passive target efficiency through experiments and Monte Carlo simulations.[178] The results showed that tumor volume could selectively change the tumor uptake of drug carriers, and the retention efficiency was dominated by the frequency of interaction and Brownian motion for smaller and larger carriers, respectively. Although concerted efforts have been made to optimize the physicochemical properties of carriers, no clear trends have depended on identifying physicochemical parameters that influence targeting efficiency.[179]

Stimulus-mediated passive target. Additionally, target sites with specific features could be used to design stimulus-mediated passive target of carriers to increase local aggregation by incorporating responsive polymers into delivery systems. Under stimulus conditions, stimulus-mediated passive target can be divided into internal stimulus-mediated passive target and external stimulus-mediated passive target.

Internal stimulus-mediated passive target exploits distinctive characteristics of the tissue microenvironment, such as pH, redox, enzyme, and temperature. The most important microenvironment feature is pH because its differentiation exists at many specific and pathological sites in the human body, such as pH 2 in the stomach, pH 9 in the intestine, pH 6.0–6.8 at the tumor site and pH 7.0–7.4 at the normal tissue, which enable the rationale for drug target administration.[85] For instance, to withstand harsh gastrointestinal conditions and prevent premature drug release, hydroxypropyl methylcellulose acetate succinate was incorporated into the middle oil phase to fabricate delivery systems.[2] The microcapsules showed no leakage at pH 1.5 and 5.5 and were released rapidly at pH 6.8 and 7.4, achieving targeted treatment of inflammatory bowel disease. In addition, the fast-growing tumor regions are always accompanied by abnormal oxygen tension, and enzyme concentration, which could be treated as the signal of carrier aggregation for passive target.[180,181] For instance, using the gradients of oxygen tension and acute hypoxia (less than 1.4% oxygen), hypoxia-targeted carriers were reported by Perche *et al.* by incorporating azobenzene with hypoxia sensitivity and specificity.[182]

Alternatively, the fascinating design involves not directly targeting the sites with a specific microenvironment but utilizing it as a stimulus to achieve flexible delivery. An example is stimulus-triggered size transition delivery systems for targeting acidic tumors[183] (Fig. 7(a)). When circulating in the blood at a neutral pH, the carrier maintained a size of 80 nm. Upon entering the tumor with a slightly acidic microenvironment, the carriers underwent a dramatic and sharp reduction in size, transitioning to less than 10 nm.

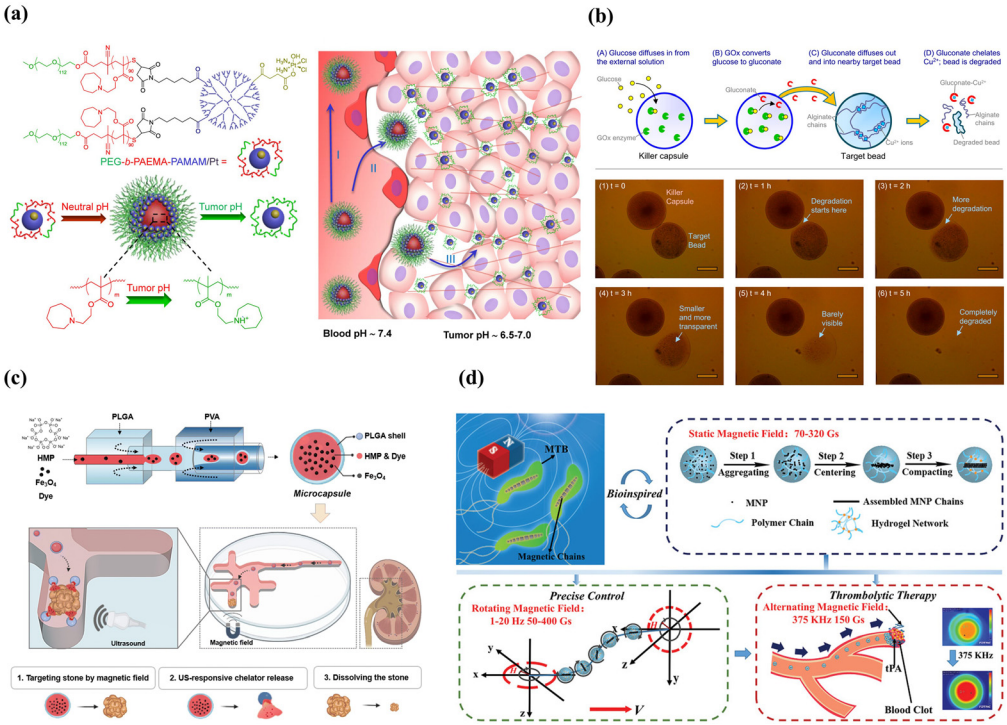

Fig. 7 Smart microcapsules with different passive target approaches. (a) Tumor-pH-triggered size transition delivery systems could overcome biological barriers to *in vivo* drug delivery in poorly permeably pancreatic tumor models. Reprinted with permission from ref. 183. Copyright 2016, American Chemical Society. (b) In the presence of a glucose environment, killer microcapsules with the enzyme glucose oxidase could continuously generate gluconate ions to chelate with copper and selectively attack the particles that were cross-linked by metal ions. Reprinted with permission from ref. 184. Copyright 2016, American Chemical Society. (c) Microcapsules loaded with Fe_3O_4 nanoparticles and hexametaphosphate exhibited efficient magnetic mobility and targeted urolithiasis-specific sites. Reprinted with permission from ref. 185. Copyright 2023, the Royal Society of Chemistry. (d) Biomimetic spherical microrobot with magneto-collective regulation for targeted thrombolysis. The aligned magnetic nanoparticle chains played the critical role of magnetic sensitivity in the propulsion of the microrobot and amplified the thrombolysis effect in a collective motion. Reprinted with permission from ref. 186. Copyright 2020, WILEY-VCH Verlag GmbH & Co. KGaA, Weinheim.

Another example involves the creation of "killer" microcapsules. As shown in Fig. 7(b), killer microcapsules are designed to selectively target and destroy targeting particles with the property of copper cations.[184]

External stimulus-mediated passive target is designed to respond to externally given stimuli, such as light, magnetic, and ultrasound.[187] Light and ultrasound stimuli play a more significant role in triggering release than accumulation at the target site. Therefore, we highlight magnetic-mediated passive target in this section. The most important step for external magnetic-mediated passive target is the incorporation of superparamagnetic nanoparticles, which enable carriers to be manipulated in a switchable magnetic field and provide accurate and efficient target delivery. By injecting chelating solution encapsulated Fe_3O_4 superparamagnetic nanoparticles into the inner core (Fig. 7(c)), double emulsion templated microcapsules exhibited efficient delivery efficiency (>90%) and target delivered to specific urolithiasis sites for urolithiasis treatment.[185] Besides, Fe_3O_4 nanoparticles could be incorporated into the capsule membrane for smart magnetic targeting.[188] An advantage of this approach is that the nanoparticles embedded in the capsule membranes did not diffuse out the membranes even after repeated swelling/shrinking 20 times. Ferrofluid was also used to functionalize the polyelectrolyte microcapsules to achieve magnetic targeting.[189] Although delivery systems with Fe_3O_4 nanoparticles can achieve site-specific targeted delivery, direction-specific delivery is restricted. By taking advantage of microfluidics, microcapsules with eccentric magnetic cores were fabricated, which enabled the microcapsules to control the specific direction *via* magnetic-guided rotation.[190] The magnetic target combined with the responsive property enables the fabrication of multi-stimulus-responsive carriers for accurate delivery. An example was thermo-responsive PNIPAM-shell embedded superparamagnetic Fe_3O_4 nanoparticles and pH-responsive microcapsules, which showed magnetic-guided targeting performance, self-regulated release according to pathological sites with different pH levels, and controlled thermo-triggered release.[188] It is noteworthy that micro/nanorobots driven by magnetic are the most promising systems for targeting delivery given their capacity for remote, precise, and non-invasive maneuvering.[191,192] As shown in Fig. 7(d), by

incorporating magnetic nanoparticles into the PEGDA and poly(ether imide) prepolymer solution, microrobots with precise magneto-collective control were fabricated.[186] With the advantage of magnetic-mediated accurate positioning control (less than 4% deviation), the microrobots navigated precisely to the target sites for ultra-minimal invasive treatment.

3.2.2 Active target delivery. Despite the passive target being extensively explored to achieve target delivery for diverse applications, the ability of these carriers to effectively target and remain at the desired sites is limited owing to multiple barriers, particularly within porous and physiological media. Active targets, incorporating target ligands on the surface of carriers, have the potential to significantly enhance targeting recognition and reduce off-target effects.[193] The key distinction between active target and passive target lies in the presence of an initial step, involving ligand-mediated recognition and affinity at target sites or not.

The common ligands for active targets include antibodies,[194] aptamers,[195] proteins,[196] peptides[197] or small molecules.[198] The conjugation of a suitable ligand endows the carriers with an efficient initial attachment and ensures the target delivery.[199] For example, by equipping with folate ligands, microcapsules show effective cytotoxic activity for cervical cells, and growth-inhibitory activity and vitro cytotoxicity are 8 times higher than the ligand-unmodified micelle.[200] Microcapsules conjugated with estrogens were fabricated to target breast cancer cells expressing estrogen receptors, and the drug uptake results were 13.9 times higher than plain drug.[201] Although single-ligand-modified carriers improve the overall target and internalization ability compared with unmodified carriers, their targeting selectivity, uptake ability and transmigration are limited by complex physiological barriers.[202–204] One potential solution is to incorporate different types of ligands within a single vehicle to create dual-targeting.[205,206] Dual-targeting carriers could be designed to target different receptors on the same cells, thereby improving the targeting selectivity.[207] For instance, by incorporating both folic acid and ABX-EGF scFv antibody to decrease off-target, microcapsules are fabricated to enhance siRNA cellular uptake and transfection efficiency. This optimized dual-ligand system exhibits 2.5- and 1.5-fold cellular activity compared to the corresponding single-modified carrier.[208] Additionally, dual-ligand targeting systems enhance internalization ability by a synergistic effect for on-target delivery.[204] For example, using folic acid as the targeting ligand for tumors and TAT as a penetrating peptide to reduce off-target transport, carriers with combinatorial ligands are fabricated using a microfluidics-assisted flow-focusing device.[209] The results demonstrate that dual-targeting carriers achieve a synergistic targeting effect for tumors, which is 3.2 times higher in tumor cell uptake compared to single folic acid-modified carriers. Alternatively, receptor-mediated targeting was integrated with environment-mediated targeting to achieve a dual targeting design for drug delivery,[210] as shown in Fig. 8(a).

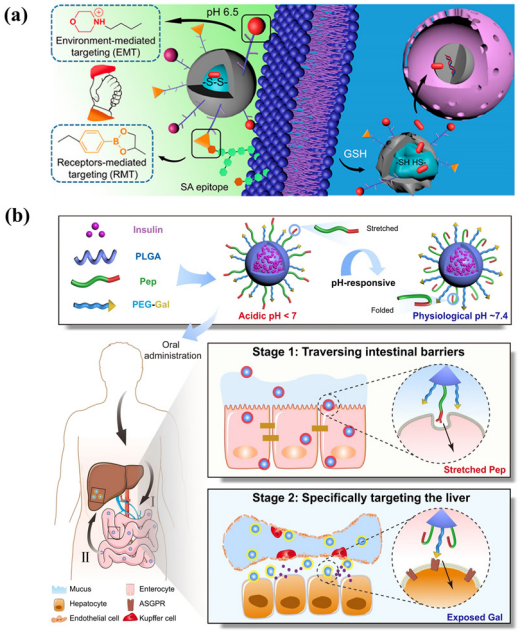

Fig. 8 Smart microcapsules with different active targeting approaches. (a) Dual targeting delivery systems engineered with phenylboronic acid and morpholine for receptor-mediated targeting and environment-mediated targeting to enhance tumor-specific sites. Reprinted with permission from ref. 210. Copyright, 2017, American Chemical Society. (b) Ligand-switchable delivery systems with a pH-triggered stretchable cell-penetrating peptide and a hepatic targeting moiety for effective diabetes management. Reprinted with permission from ref. 211. Copyright 2022, Springer Nature.

However, the effectiveness of carriers with dual-ligand targeting systems is not always enhanced owing to the influence of different formulations and the potential mutual interference between diverse ligands.[212] It is critical to optimize synergetic combinations and minimize mutual interference between ligands to achieve effective active target delivery.[213] One powerful strategy is to adjust varied parameters of ligands, including the density, ratio, and relative length.[214] Increasing ligand density does not always result in a higher cellular association, as there exists an optimum number and minimum threshold for a better targeting outcome, which can be determined using particle counting techniques.[215,216] Additionally, the ratio and relative length of ligands can influence conformation and mobility and consequently affect their targeting ability. For example, using a flow-focusing microfluidics device, Liu *et al.* fabricated a combinatorial library of single- and dual-ligand microcapsules to systematically study the effects of ligand targeting efficiency.[217] The results showed that the dual ligand did not show a targeting effect using folic acid with a 5 K molecular weight and hyaluronic acid with either 5 K or 10 K, and the synergetic effect was enhanced when using hyaluronic acid with 7 K. An alternative strategy to enhance target selectivity is combining heterogeneous ligands, such as

stimulus-responsive actuator,[218] copolymer,[219] and Janus structures.[220] As shown in Fig. 8(b), ligand-switchable carriers were fabricated by introducing cell-penetrating peptides for pH-responsive conformational changes and the Gal moiety to target liver.[211] After oral administration, in acidic environments, the peptide maintained a stretched state facilitating efficient transport in the intestine, and upon entering physiological pH, the peptide made a conformational change, which contributed to Gal exposure and promoted hepatic glycogen production by 7.2-fold for insulin therapy.

3.2.3 Microfluidics-assisted target. Microfluidics can enhance target capture and recognition for efficient enrichment by improving the encounter rate and augmenting the kinetics and thermodynamics of the microfluidics affinity interface.[221] Although microfluidics-assisted target is mainly applied to cell recognition and aggregation, it has great potential for carriers to achieve target delivery.

The microfluidics fluid is dominated by a laminar fluidic pattern, which limits the encounter rate between the target and recognition sites. The microfluidics platforms designed with a high surface/volume ratio, including high-aspect-ratio microchannel chip,[222] micropillar array chip,[223] micromixing chip,[224] and 3D nanoporous chip,[225] have been introduced to enhance the encounter rate. For example, a size-dictated immunocapture chip based on deterministic lateral displacement was designed using hydrodynamically optimized triangular micropillars.[226] In this microchip (Fig. 9(a)), larger particles exhibited more frequent interactions with micropillars than smaller particles. This facilitated the size-based selection of circulating tumor cells, which are larger than blood cells. Additionally, a clockwise rotation of a triangular micropillar by 15° around its axis amplified adhesion force gradients and diminished hydrodynamic force gradients, which enabled the efficient enrichment of the target cells. To enhance mass diffusion, the herringbone as the microvortex-generator was introduced to design a microvortex mixing chip for efficient tumor cell aggregation (Fig. 9(b)). The herringbone chip showed a capture efficiency of 91.8% for tumor cells, achieving a 26.3% improvement compared to the control.[227]

Alternatively, the microfluidics substrate could be modified with recognition molecules to enhance the interface affinity. For instance, aptamer-functionalized leukocyte membrane nanovesicles were combined with a microfluidics chip to achieve enrichment of circulating tumor cells, as

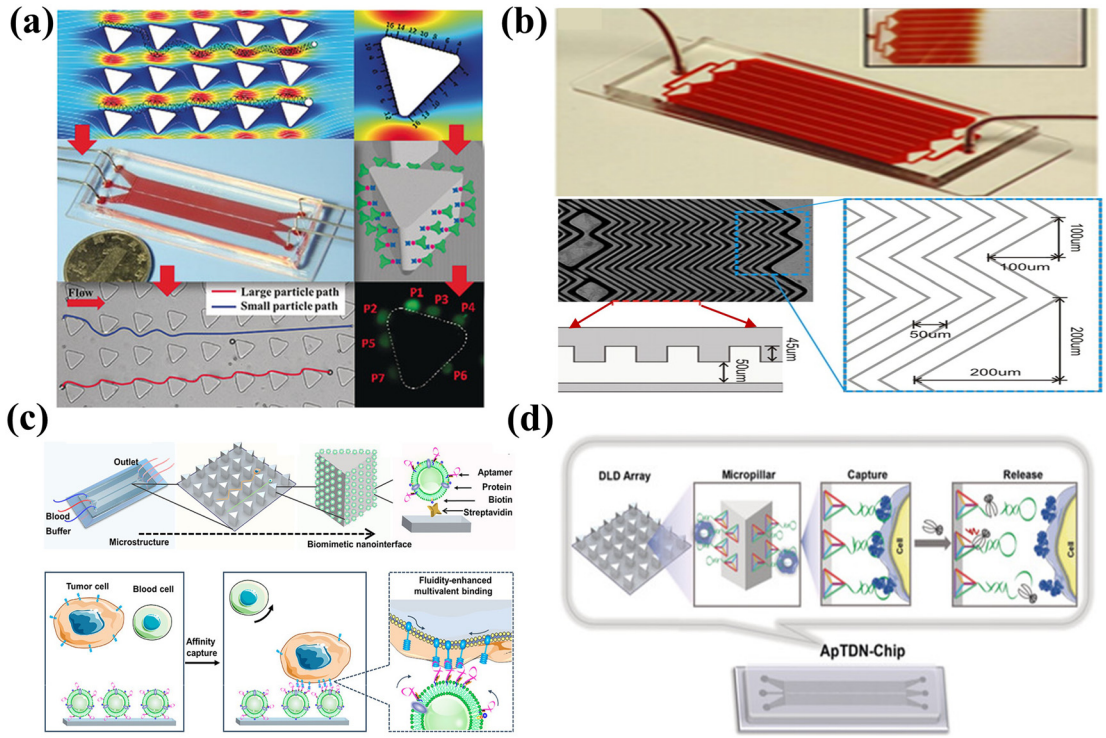

Fig. 9 Microfluidics-assisted targeting chips. (a) Size-dictated immunocapture chip with rigorous computational analysis of various parameters and immobilized antibodies on the surface of each micropillar. Reprinted with permission from ref. 226. Copyright 2017, Wiley-VCH Verlag GmbH & Co. KGaA, Weinheim. (b) Herringbone chip with herringbone-induced microvortices disrupted and increased the number of cell–surface interactions in the antibody-coated device. Reprinted with permission from ref. 227. Copyright 2010, *Proceedings of the National Academy of Science of the United States of America*. (c) Fluidic multivalent microfluidics chip with aptamer-functionalized leukocyte membrane nanovesicles and soft and high-affinity nanointerface for high-performance isolation of circulating tumor cells. Reprinted with permission from ref. 228. Copyright 2020, American Chemical Society. (d) DNA nanolithography in a microfluidics chip decorated with sub-10 nm three-dimensional DNA structures as frameworks with a pendant aptamer at the top vertex for effective recognition. Reprinted with permission from ref. 229. Copyright 2020, Wiley-VCH Verlag GmbH & Co. KGaA, Weinheim.

shown in Fig. 9(c). The fluidic multivalent nanointerface contributed to high affinity binding with circulating tumor cells and exhibited low absorption of background blood cells.[228] Besides, the soft and flexible nanovesicles between the cell and the capture substrate acted as a cushion and could reduce cell damage caused by interfacial collisions. The modified microfluidics chip demonstrated a substantial affinity enhancement of 4 orders of magnitude and exhibited a capture efficiency that is 7 times higher than that of a chip functionalized with monovalent aptamers. Although numerous manufacturing methods have been devised for micro-scale structures, it is still a technical challenge to achieve reproducible preparation of nano-scale structures with highly precise dimensions. The "DNA nanolithography in a microfluidics chip" introduced by Zhang *et al.* providing an alternative approach for the fabrication and cost issues of microfluidics chips,[229] as shown in Fig. 9(d). The sub-10 nm tetrahedral DNA nanostructure-17 was attached to the microfluidics substrate as the rigid framework, and aptamer SYL3C as the recognition element was assembled at the top vertex of the DNA fragments instead of directly attaching the aptamer to the microfluidics substrate. The tetrahedral DNA nanostructures facilitated the upright-oriented anchoring of recognition molecules, avoiding crowding effects and achieving an enhanced accumulation efficiency of up to 60%.

4. Microfluidics-assisted smart microcapsules for controlled release

After arriving at the designated location, the controlled release of encapsulants across the membranes is the necessary step for final delivery. The definition of controlled release provided by the European Directive (3AQ19a) is the distribution of encapsulants at a specified time interval when a particular stimulus is encountered.[230] The fundamental mechanisms of controlled release are essential to be studied for designing the release profiles and release procedures. In this chapter, the release mechanisms are used as the starting point to present the controlled release procedures adjusted by the smart whole membrane and smart on/off gates and release kinetics.

4.1 Release mechanisms

The release mechanism is of great importance in defining release profiles and even governs the release rate. Several release mechanisms have been introduced,[230] as depicted in Table 5. It is essential to note that there is no clear independence between the different release mechanisms and often a combination of these mechanisms establishes the release of encapsulants. Based on different release mechanisms, there are different types of release profiles. According to the release time, the basic release profiles can be classified as burst release and sustained release.[231] Through the flexible combination of the two basic release profiles, the programmed sequential release can be designed for controlled release.

4.2 Smart microcapsules for controlled release

Under specific conditions, stimuli induce conformational transitions in the barrier shells of smart microcapsules at the microscopic level. Subsequently, the membranes amplify the conformational transitions into macroscopically measurable changes in the barrier properties.[29] We summarize the common stimulus-triggered release mechanisms, as presented in Table 6. The responsive barrier shell could employ whole membranes or smart "gates" on the shell to achieve controlled release.

4.2.1 Smart microcapsules with membrane-based rupture for burst release. The release mechanisms, including dissolution, disintegration, swelling and osmosis, contribute to the membrane-based rupture, leading to burst release. Changes in membrane-based rapture are grouped into chemical and physical changes.

Chemical changes include the chemical cleavage of cross-links and trigger depolymerization. For example, microcapsules with cytosine-rich shells cross-linked by nucleic acid bridges can undergo cleavage at pH 5.0, leading to shell decomposition and pH-triggered release of encapsulants.[237] Using polyphenol tannic acid as the crosslinker to fabricate supramolecular microgel, the resultant smart microgel exhibited pH-responsive burst release owing to deprotonation-induced disintegration at high pH.[238] In addition, pH-enzyme-delayed colon-targeting

Table 5 Summary of release mechanisms and properties for controlled release

Release mechanisms	Release properties
Diffusion	The most preponderant mechanism; the concentration gradient as the driving force; the pore size is large enough to allow the encapsulants to transport
Dissolution/melting	Membrane-based disintegration, easy to design; starting from outside the carriers and progressing to the inside
Disintegration	Membrane-based disintegration, cleavage of cross-links, triggered depolymerization, mechanical-induced degradation
Swelling/shrink	Membrane-based permeability alteration even breaks the shell and solvent absorption
Osmosis	Membrane-based permeability alteration even breaks the shell, selectively water-permeable of the carrier

Table 6 Summary of the common stimulus-triggered release mechanisms for controlled release

Structures	Key materials	Stimuli	Release mechanisms	Ref.
W/O/W	Phosphate buffered saline solution/toluene, chloroform, PLGA, gold nanorods/2 wt% PVA	Light	Near infrared-induced melting	95
W/O	4 wt% biocide, 40 wt% PEGDA, 1 wt% photoinitiator, fluorescein sodium salt/98 wt% dodecane, 2 wt% EM 90	Water	Stimulus-induced swelling	104
W/O/W	Sucrose, 3 wt% PVA /poly(ethylene glycol) divinyl ether, trimethylolpropane tris(3-mercapto propionate), dichloromethane/$CaCl_2$, 10 wt% PVA	Osmotic pressure	Pressure-induced rupture	133
W/O/W	5 wt% PVA/poly(phthalaldehyde), chloroform/10 wt% PVA	Fluoride	Stimulus-induced depolymerization	232
W/O/W	5 wt% PVA /acrylic acid, methyl methacrylate, 70 vol% chloroform, 30 vol% tetrahydrofuran/10 wt% PVA, 15 wt% tetrahydrofuran	pH	Stimulus-induced dissolution	233
W/O/W	Zonyl-FSO 100/perfluorohexane Zonyl-FSO 100/10 wt% PVA	Ultrasound	Acoustic vaporization-induced rupture	234
(W/O)/W/O	Nanoparticles/1% w/v Pluronic F127, NIPAM, *N*,*N*-methylene bisacrylamide, 2,2′-azobis(2-amidinopropane) dihydrochloride/soybean oil, 8 w/v% PGPR 90	Temperature	Stimulus-induced shrinking	117
W/O/W	2 w/w% PVA, sodium chloride-poly(*N*,*N*-diethylacrylamide), benzophenone, chloroform-2 w/w% PVA, sodium chloride	Temperature	Stimulus-induced dissolution	235
W/O/W	Glycerol/fatty glycerides/glycerol, PVA	Temperature	Stimulus-induced melting	114
W/O/W/O	Aqueous solution containing hydrophilic actives/hexadecane/10% PEGDA, 2% PVA, and photoinitiator/2% Span 80, mineral oil	Mechanical pressure	Stimulus-induced rupture	116
W/O/W	10 wt% PEG/chloroform, hexane, PEG-*b*-poly(lactic acid) (PLA), PNIPAM, PLGA, dodecyl thiol-stabilized gold nanoparticles/10 wt% PVA	Light and temperature	Stimulus-induced dissolution and melting	157
W/O/W	Graphene oxide suspensions/amodimethicone (KF 860), a diamino-modified polymeric silicone, silicone oil/80 wt% glycerol, 1 wt% PVA	Light and magnetic	Light-induced melting	236
O/W/O	Soybean oil, glutaraldehyde/chitosan, *N*-isopropylacrylamide, iron(III) chloride/-soybean oil, glutaraldehyde	pH, temperature, magnetic	Stimulus-induced swelling and shrinking	188

delivery has been produced through shell degradation, in which around 20% of the protein was released in the stomach and small intestinal fluid and about 58% was released in the colon fluid containing β-glucosidase.[110] Additionally, carriers with depolymerizable membranes offer tunable trigger release by depolymerizing the shell under the desired stimuli. Using poly(phthalaldehyde) as a depolymerizable polymer, fluoride-responsive microcapsules were fabricated, in which fluoride exposure led to the breaking of end-caps, rapid depolymerization from head-to-tail, and release of encapsulants.[232] The nitric oxide (NO) expression increases along with intestinal inflammation and can be used to design NO-responsive delivery by embedding probiotics into poly-γ-glutamic acid microcapsules. As shown in Fig. 10(a), the dissociation of the shell was accompanied by the transformation of NO into dinitrogen trioxide and an irreversible reaction with the cross-linking agent *o*-phenylenediamine, enabling the rapid release of probiotics in response to NO.[239]

The physical changes, including swelling/deswelling or osmosis-induced rupture, melting/dissolution-induced decomposition, and mechanical-induced fragmentation, offer an alternative strategy for trigger release, avoiding the need for complex shell synthesis with multiple functionalities. For example, hydrogel-based shells with water-triggered release were created, in which water absorption caused the hydrogel to swell by approximately 40%, leading to the release of encapsulated biocide.[104] Using the property of osmosis to increase the size of the membrane and thickness, submillimeter capsules with ultrathin shells (0.83–2.80 um) were fabricated and easily compressed to rupture, releasing the encapsulant for cosmetic applications.[241] Inspired by the squirting plants ejecting seeds, microcapsules with PNIPAM-based shells were produced and achieved thermo-triggered squirting release, which could shrink and rupture at higher temperatures because of increased internal pressure.[117] Using palm oil-based shells, the thermos-responsive carriers exhibited burst release of the aqueous core when the temperature was above the melting point 38 °C,[240] as shown in Fig. 10(b). By incorporating shellac polymer into the shell, the microcapsule with pH-triggered release was fabricated because the carboxylic groups were ionized, and the shell eventually dissolved at alkaline pH for targeted intestinal release.[67] An interesting design was using thermally induced microcracks to release active materials for fabricating amino-functionalized membranes applied in heavy metal ion removal.[242]

Traditional single stimulus-triggered microcapsules often exhibit burst release, which may not be suitable for certain applications, such as oral administration. It is crucial to develop microcapsules with multiple stimuli. This can be achieved by incorporating multiple stimulus-responsive materials or particles into the polymeric shell. For instance, photo- and thermo-responsive polymersomes were created by embedding photothermal gold nanoparticles into a thermosensitive polymeric membrane.[157] Similarly, multi-

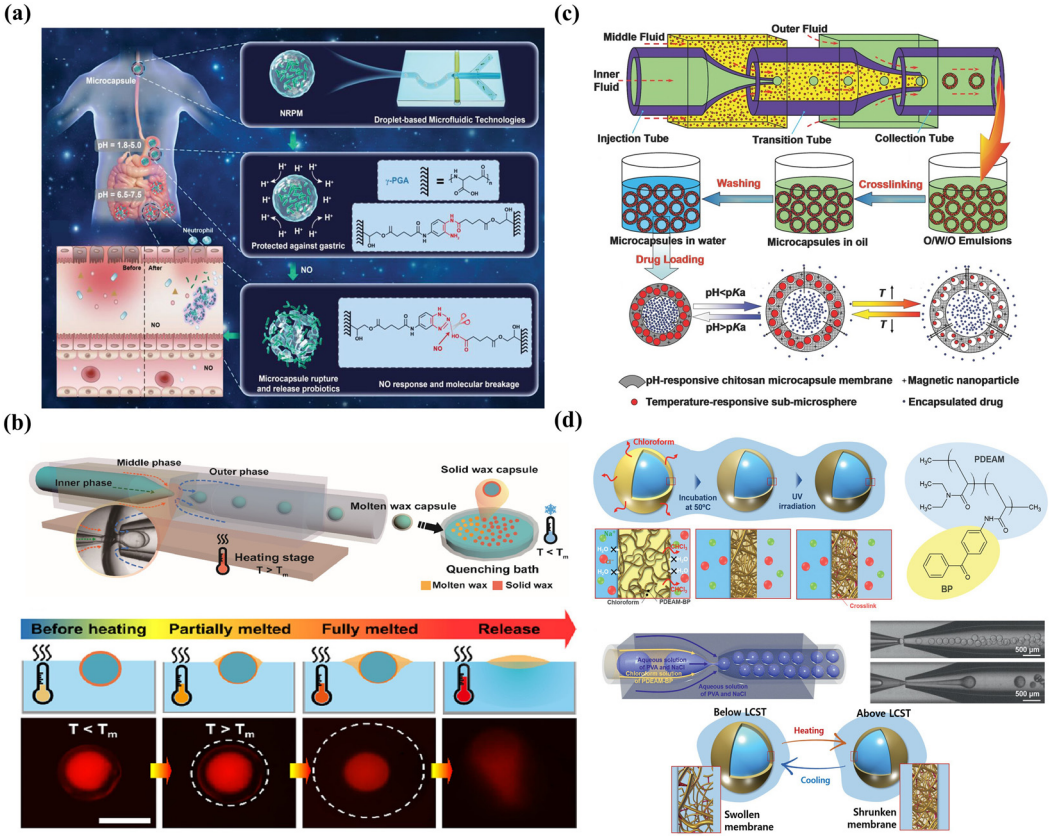

Fig. 10 Smart microcapsules with membrane-based controlled release. (a) Smart microcapsules with NO-induced chemical dissociation for burst release. Reprinted with permission from ref. 239. Copyright 2022, Wiley-VCH GmbH. (b) Smart microcapsules with temperature-induced physical melting for burst release. Reprinted with permission from ref. 240. Copyright 2021, American Chemical Society. (c) Smart microcapsules with multiple stimuli (pH, temperature, and magnetic field) for controlled release. Reprinted with permission from ref. 188. Copyright 2014, WILEY-VCH Verlag GmbH & Co. KGaA, Weinheim. (d) Smart microcapsules with membrane-based thermo-responsive permeability alteration for sustained release. Reprinted with permission from ref. 235. Copyright 2021, Wiley-VCH GmbH.

stimulus-responsive microcapsules were fabricated by first constructing a pH-responsive chitosan crosslinked membrane and then incorporating magnetic nanoparticles and acrylamide sub-microspheres into it, as shown in Fig. 10(c).[188]

4.2.2 Microcapsules with membrane-based permeability alterations for sustained release. It is of great importance to maintain encapsulated active materials at a certain concentration and predetermined rate for a long time instead of burst release, especially for drug administration.[243] Carriers for sustained release are typically designed with tunable permeability membranes that act as gatekeepers for controlled diffusion in and out. Directly fabricating the membrane as a diffusion barrier is a simple method for achieving sustained release. In addition, the release mechanisms that lead to changes in mesh size, including swelling, osmosis, and partial degradation, contribute to membrane-based permeability alteration for sustained release.

Directly fabricating the membrane as a diffusion barrier can affect the diffusion rate of the encapsulants and thus achieve sustained release. Notably, adjusting the shell thickness is a simple method for controlling sustained release. For example, by adjusting the concentration of monomer, the thickness was adjusted from 70 to 150 nm, and the period of sustained release was controlled from 3 to 5 months.[244] Biodegradable shells, such as biodegradable materials PLA,[245] PLGA,[244] and paclitaxel,[246] were also used to control the shell thickness and thus affected the diffusion rate of the encapsulants for sustained release. During degradation, local environmental conditions, such as pH, influence the degradation rate and need to be considered.[247] It is worth mentioning that the core component can increase the diffusion path and thus prolong the release time of encapsulated substances. As reported by Kim *et al.*, microcapsules with a hydrogel core exhibited no release for the initial few minutes, while the control group without a hydrogel core immediately released half of the encapsulants in 35 s.[248] Owing to the outstanding ability of water adsorption, the hydrogel is a good candidate for the membrane material for sustained release.[249] Although the inherent network structures of hydrogels with large mesh sizes are capable of molecular exchanges, hydrogel microcapsules are poorly suited for the release of small molecules for sustained release. To solve this question, Hu *et al.* fabricated microcapsules with two distinct layers of

shells, achieving remarkable slow release for the hydrophilic small molecule rhodamine 6G.[250]

The combination of functional materials with stimulus-induced conformational change and permeability alteration of membrane endows carriers with the tunable cut-off threshold for size-selective permeation. The permeability could be changed by recognizing different stimuli, such as pH,[251] temperature,[188] and light.[252] As shown in Fig. 10(d), using poly(*N*,*N*-diethylacrylamide) with volume phase transition temperature (VPTT) property as the middle phase, the degree of swelling gradually decreased as the temperature increased, which made a collapsed network with a small mesh size and low permeability.[235] Quantitatively, the mesh size of the membrane was between 2.8 nm and 4.6 nm at 4 °C and 25 °C owing to the temperature-dependent change in permeability, respectively. The cutoff threshold of the membrane can be controlled by adjusting the molar mass of the functional monomer.[253] In theory, factors affecting the change in VPTT could be used to control the swelling and shrinking of thermo-responsive polymers and thus control permeability. Based on this, glucose-responsive microcapsules were produced. Zhang *et al.* adopted 3-acrylamidophenylboronic acid acting as the glucose sensor, and the charged form was capable of stable complex formation with glucose, which changed the dissociation equilibrium and shifted the VPTT of PNIPAM to a higher temperature, resulting in glucose-induced swelling.[78] Alternatively, by pH-induced protonation/deprotonation of the polyelectrolytes, swelling/shrinking changes in the membrane could be responsible for controlling permeability.[254] An interesting design was to use polyacrylic acid with a pH-responsive swelling property to fabricate a booster chamber that provided a driving force for the release of the drug chamber.[255]

The greatest advantage of membrane-based permeability alteration is that it can avoid the irreversible change and structural damage of shells compared to membrane-based rupture, which is of great importance when designing reversibly and dynamically tunable release. As shown in Fig. 11, using thiol-ene polymerization, poly(anhydride) microcapsules were fabricated and then hydrolyzed in its aqueous environment, yielding cross-linked poly(acid) microcapsules with tethered carboxylic acids, which rendered the microcapsules with pH-responsive property. More importantly, the deprotonation at high pH of the anhydride increased the mesh size and hydrophilicity of the membrane, increasing the permeability and leading to the membrane's nondestructive and reversible swelling.[256,257] In addition, the dynamic membrane could switch numerous times between impermeable and permeable even after drying in the vacuum at room temperature.

4.2.3 Combined release profiles for programmed sequential release. Although smart microcapsules achieve controlled release under different stimuli conditions and expand the application fields, they may not meet the requirements of controlled sequence release for special conditions.[258] Despite controlling shell thickness by providing a straightforward method for sequential release, it delayed the release time from 2 min to 15 min along with the shell thickness from 500 nm to 4 μm.[233] It is of great importance to fabricate microcapsules with programmed sequential release through a flexible design and combined release mechanisms.

Typically, programmed sequence release could be achieved by engineering smart microcapsules with a core–shell structure or multi-compartment combined with different release mechanisms. As shown in Fig. 12(a), nano-in-micron microcapsules with burst-sustained release were designed by encapsulating free drugs in the shell and drug-loaded nanoparticles in the core.[2] The free drug could be rapidly released owing to the decomposition of the chitosan shell,

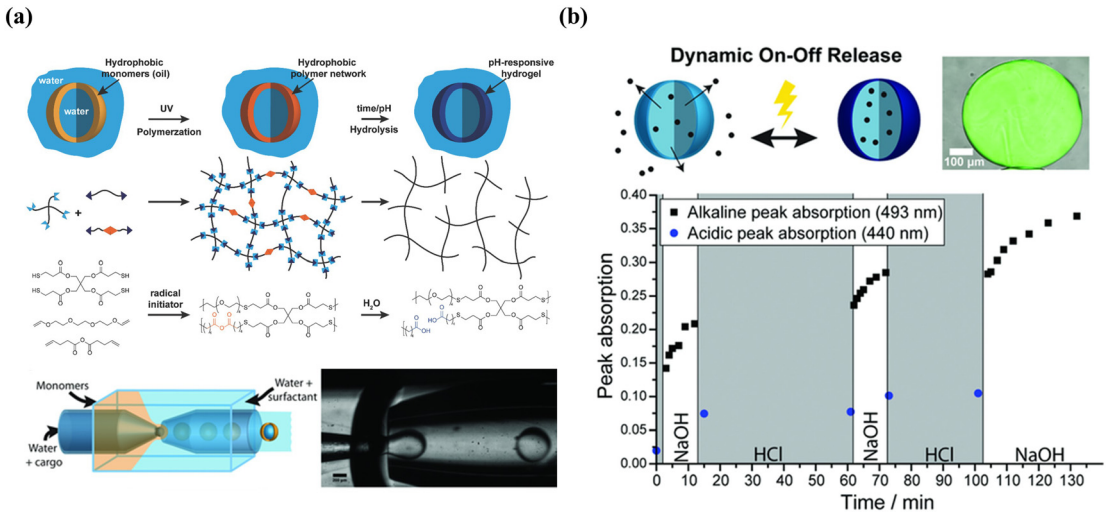

Fig. 11 Microcapsules with reversible permeability switching for sustained release. (a) Mechanism of thiol-ene-based membrane and microfluidic-assisted production of poly(acid) microcapsules (b) illustration of dynamic on–off release and time-resolved peak absorption in acidic and alkaline conditions. Reprinted with permission from ref. 256. Copyright 2018, WILEY-VCH Verlag GmbH & Co. KGaA, Weinheim.

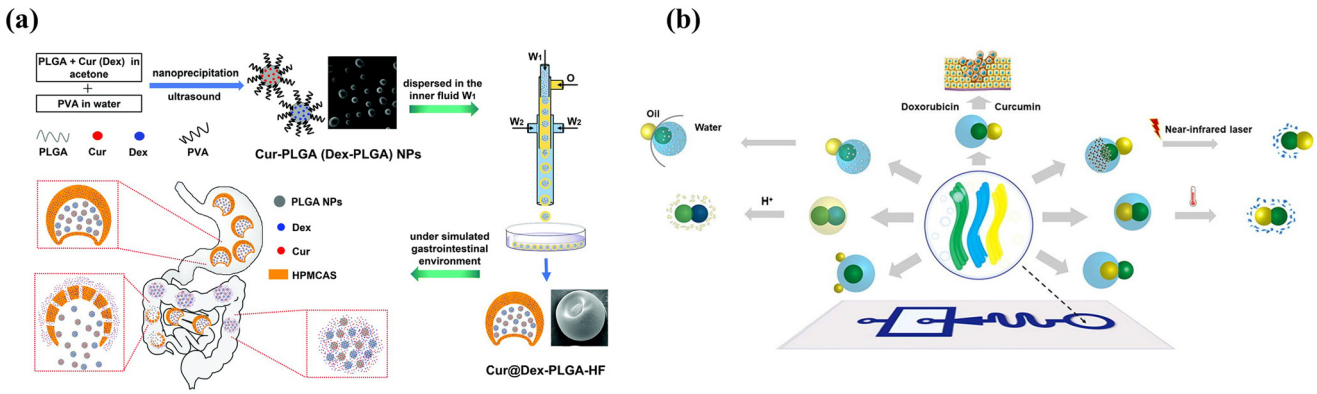

Fig. 12 Combined release profiles for programmed sequential release. (a) Microcapsules with a core–shell structure for sequential burst-sustained drug release from different compartments. Reprinted with permission from ref. 2. Copyright 2021, Royal Society of Chemistry. (b) Multiphasic Janus microparticles fabricated by applying the microfluidics phase-separation method to complicated structures to achieve programmed degradation and release. Reprinted with permission from ref. 96. Copyright 2022, Elsevier B.V.

while the drug-loaded PLGA nanoparticles provided a second and sustained release owing to PLGA degradation. Another approach to sequence release is utilizing multi-compartment microcapsules. Xu *et al.* developed pH- and temperature-responsive microcapsules with hydrophobic contents in the shell and hydrophilic contents in the core, achieving sequential release along with different stimuli.[160] Considering the smart microcapsules with multi-compartment for programmed sequence release, capsule-in-capsule structures (outer chitosan shell and inner PEGDA shell) were fabricated and achieved the first acid-triggered burst release and followed sustainable release.[66] Similarly, a polymersome-in-polymersome with a PEG-*b*-PLA diblock-copolymer bilayer was produced to achieve programmable release. The use of a PLA-homopolymer-loaded bilayer as the outer membrane allows for the sequential rupturing of membranes from the innermost to the outermost, controlling the release of core materials.[154] Incorporating PLA homopolymers into the bilayer increases mechanical and chemical stability, preventing membrane rupture even under high osmotic shock. By the advantage of Janus microparticles created with complicated structures by phase separation, multiphasic Janus systems with different degradation properties achieved zonal drug loading and programmed release. As shown in Fig. 12(b), phase transition materials were introduced into different inlets to fabricate droplets and followed changing structures by adjusting the interfacial tension in the microfluidics system, which enabled programmed degradation and release.[96]

4.2.4 Smart microcapsules with gate-based controlled release. Microcapsules with smart on/off gates are generally fabricated by "grafting-to" and "grafting-from" methods using smart polymer materials or microspheres as smart gates.[193] The resultant substrates of the microcapsule have no environmental response, and the controlled-release properties only depend on the abrupt positively- or negatively-responsive gates. Positively responsive gating increases permeability when encountering a stimulus, whereas negatively responsive gating shows reversed properties.

Depending on whether the gate materials are incorporated after or during membrane formation, the fabrication approaches for smart gates can be classified into two classifications: "grafting" techniques and "blending" techniques. Although a concentrated effort has been made to highlight smart gating membranes by bulk grafting or blending,[259–261] only few articles have focused on microfluidics-assisted smart gating membranes for controlled release. One point that needs to be clarified in advance is that porous microcapsules are not the focus of this section although they may be referred to as smart gating porous particles in other papers.[31] Considering that the bulk blending process could be segregated in confined spaces, such as a thin middle layer of emulsion droplets fabricated by microfluidics, it would be possible to construct microcapsules with smart gates. An example is the microfluidically prepared W/O/W emulsion templated smart microcapsules with molecular polarity- and temperature-dependent permeability fabricated by Kim *et al.*[262] By blending a ternary mixture of dodecanol, lauryl acrylate (LA), and trimethylolpropane ethoxylate triacrylate (ETPTA) as the middle oil phase, LA and ETPTA formed a polymeric framework upon photopolymerization, while continuous voids were filled with liquid dodecanol. Continuous dodecanol worked as the smart gate and selectively allowed molecular soluble in molten dodecanol to diffuse across the membrane when above the melting point of dodecanol. Similarly, using dodecanol continuous nanochannels to serve as smart gates for transmembrane transport (Fig. 13), smart microcapsules showed a high performance of photothermal heating upon near-infrared laser irradiation, attributed to polydopamine nanoparticles in the core and achieved on-demand drug release.[263]

4.3 Release kinetics

By investigating the release kinetics, it is possible to control and design the optimal release of encapsulants for target

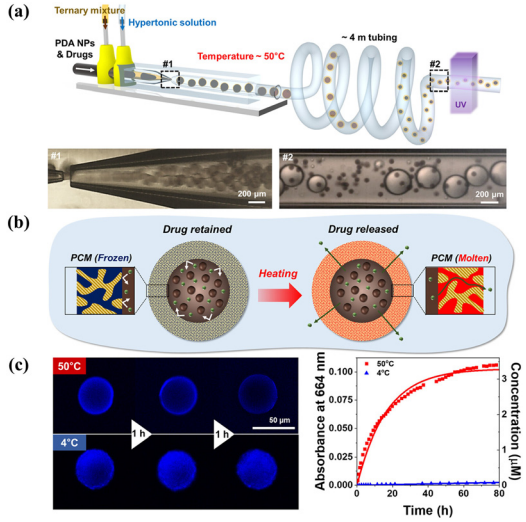

Fig. 13 Microfluidics-assisted microcapsule membrane with smart on/off gates for controlled release. (a) Schematic illustration and microfluidics device for the synthesis of smart microcapsules with on/off gates. (b) Schematic for the smart gates for on/off state responsive to temperature to achieve controlled release. (c) Confocal laser scanning microscope images and absorbance at 664 nm of methylene blue showing the release at 50 °C and no release at 4 °C. Reprinted with permission from ref. 263. Copyright 2023, American Chemical Society.

delivery. Various factors influence the release kinetics of microcapsules, including production conditions and morphology. For example, different production methods, such as microfluidics and bulk fabrication, lead to distinct release kinetics. Microfluidics-made microcapsules exhibit slower initial bursts and release rates compared to conventionally made microcapsules owing to their uniform size distribution.[103] Size and size distribution also play significant roles. Larger microcapsules with a fine size distribution show reduced initial bursts and longer release processes compared to smaller ones, attributed to longer diffusion routes and smaller surface-to-volume ratios.[264,265] Furthermore, the structure and morphology affect the release kinetics. Core–shell microcapsules exhibit higher initial release rates compared to single-layer microparticles with the same encapsulated diameter likely owing to the larger surface area-to-volume ratio of core–shell structure.[108] Different compartments within microcapsules exhibit varying release kinetics, with slower release rates observed in interior compartments compared to the outer shell, influenced by physical osmotic pressure and diffusion distance.[160] Additionally, the configurations of microcapsule shells, such as the thickness and surface coverage of pores, affect release kinetics, with thicker membranes and smaller pore surface coverage exhibiting higher burst releases and shorter release times.[85]

Mathematical models are extremely helpful for release kinetics because they can predict the release process before the target sites and measure important physical parameters, which makes them widely implemented in different target delivery kinetics.[266] Various mathematical equations are used to describe the kinetic release of active materials, as shown in Table 7. Among these kinetic equations, zero-order,[267] first-order,[268] and Higuchi models[269] are the most commonly used. For instance, alginate microcapsules encapsulating the citral exhibited a release profile well described by the first-order model, enabling sustained release.[76] Biodegradable microcapsules with hydrophilic bioactives exhibited long-term release as the membranes degraded, fitted with a biexponential function.[244] However, owing to the complexity and susceptibility to relevant factors, no single equation is universally accepted to accurately describe release kinetics.

Table 7 Summary of the commonly used kinetic models

Kinetic release models	Mathematical equations
Zero-order	$Q = Q_0 + k \times t$
First order	$Q/Q_0 = 1 - e^{(-k \times t)}$
Higuchi	$Q = k \times t^{\frac{1}{2}}$
Hixson–Crowell	$Q_0^{\frac{1}{3}} - Q^{\frac{1}{3}} = k \times t$
Korsmeyer–Peppas	$Q/Q_0 = k \times t^n$
Weibull	$Q/Q_0 = 1 - e^{-b \times t \wedge \alpha}$
Baker–Lonsdale	$\left(1 - (1 - Q/Q_0)^{\frac{2}{3}}\right) \times Q/Q_0 = 2/3 \times k \times t$
Hopfenberg	$Q/Q_\infty = 1 - (1 - k \times t)^3$
Gompertz	$Q/Q_0 = e \wedge (\alpha \times e^{\beta \log t})$

Q is the amount of released encapsulants at time t; Q_0 is the initial amount of encapsulants in the solution; k is the release constant; n characterizes the release mechanism; T accounts for the lag time; α denotes a scale parameter that describes the time dependence; and β describes the shape of the dissolution curve progression.

5. Conclusions and outlooks

In conclusion, for a smart microcapsule, an important step is not only the selection of an encapsulation carrier for the entrapment according to final applications but also the target delivery and controlled release, including sites and modes of release. Droplet-based microfluidics provides the most effective approach for fabricating microcapsules owing to its precisely manipulating fluids on the low-energy-demand micrometer scale. In this review, we discussed microfluidics-assisted microcapsules from droplet fabrication and carrier systems to target delivery and controlled release. Despite significant progress made in exploring smart microcapsules, further efforts are needed to endow microcapsules with high throughput productivity, excellent mechanical properties, outstanding active targeting functionality, and manageable release performance.

First, achieving "smart targeting" stands as a crucial aspect of microcapsule target delivery. Although considerable efforts have focused on enhancing targeting efficiency through external forces, such as magnetic or electronic fields, relatively limited emphasis has been placed on active targeting *via* host–guest or ligand–receptor chemistry. External stimuli, such as gradient diffusion in concentration or temperature, also hold promise for inducing target delivery. However, there are very few examples of "robot-based" delivery, leveraging intelligence for target localization

and cargo delivery. Thus, the integration of artificial intelligence is imperative to streamline robot design and fortify the fabrication of robot-based delivery strategies. Moreover, machine learning stimulates the design and screen ligands to facilitate target delivery efficiently.

Second, the realm of production rate enhancement presents substantial opportunities. Despite advancements in microfluidics techniques, such as parallel or multi-layer devices, bolstering the production rate of smart microcapsules remains constrained, particularly in practical fields such as enhanced oil recovery due to extensive particle demand. Moreover, the current high throughput devices mostly increase the single emulsion templated microcapsule production rate, which is somehow limited by "smart" performance owing to shell material compromise. There are few examples in the literature of industrial applications to generate multi-compartment microcapsules or microparticles using high-throughput devices. Leveraging computer science and trainable statistical models, machine learning has emerged as a pivotal tool for prognosticating droplet generator performance and flow patterns based on design parameters. This capability curtails expensive design iterations and bridges the knowledge gap between experts and end-users. Machine learning exhibits immense potential in automating microfluidics design, optimizing operations, and facilitating the scaling up of production systems, thereby achieving high-throughput production.

Finally, to heighten loading efficiency, a promising solution involves combining droplet-based microfluidics technology with diverse self-assembly methods, such as supramolecular host–guest chemistry. Furthermore, prevailing studies on microcapsules equipped with smart gates predominantly depend on multi-step synthesis processes, which often compromise encapsulation efficiency. Alternatively, the combination of bulk nanoparticles with microfluidics-assisted emulsification has substantial potential for target delivery and quantitative release. Overall, the fabrication of smart microcapsules exhibiting active target performance, possibly crafted into artificial intelligence particles, envisages various practical applications.

Conflicts of interest

The authors declare no competing financial interest.

Acknowledgements

The authors thank the National Natural Science Foundation of China Project (ZX20210340), National Talent Support Project (ZX20220351), Shandong Province Innovative Team and Talent Project (ZX20230148) and Research start-up funding projects of China University of Petroleum (East China) (20210085) for financial support. The support from the Oil and Gas Field Chemistry Institute, School of Petroleum Engineering, China University of Petroleum (East China) is also appreciated.

References

1 S. S. Datta, A. Abbaspourrad, E. Amstad, J. Fan, S. Kim, M. Romanowsky, H. C. Shum, B. Sun, A. S. Utada, M. Windbergs, S. Zhou and D. A. Weitz, *Adv. Mater.*, 2014, **26**, 2205–2218.
2 J. Jiang, J. Xiao, Z. Zhao, M.-S. Yuan and J. Wang, *Mater. Chem. Front.*, 2021, **5**, 6027–6040.
3 T. Moragues, D. Arguijo, T. Beneyton, C. Modavi, K. Simutis, A. R. Abate, J. C. Baret, A. J. deMello, D. Densmore and A. D. Griffiths, *Nat. Rev. Methods Primers*, 2023, **3**, 1.
4 L. Shang, Y. Cheng and Y. Zhao, *Chem. Rev.*, 2017, **117**, 7964–8040.
5 W. Wang, B.-Y. Li, M.-J. Zhang, Y.-Y. Su, D.-W. Pan, Z. Liu, X.-J. Ju, R. Xie, Y. Faraj and L.-Y. Chu, *Chem. Eng. J.*, 2023, **452**, 139277.
6 T. Takei, Y. Yamasaki, Y. Yuji, S. Sakoguchi, Y. Ohzuno, G. Hayase and M. Yoshida, *J. Colloid Interface Sci.*, 2019, **536**, 414–423.
7 W. Wang, R. Xie, X.-J. Ju, T. Luo, L. Liu, D. A. Weitz and L.-Y. Chu, *Lab Chip*, 2011, **11**, 1587–1592.
8 A. G. Skirtach, A. M. Yashchenok and H. Möhwald, *Chem. Commun.*, 2011, **47**, 12736–12746.
9 T. Li, D. Teng, R. Mao, Y. Hao, X. Wang and J. Wang, *J. Biomed. Mater. Res., Part A*, 2019, **107**, 2371–2385.
10 J. L. de Oliveira, L. F. Fraceto, A. Bravo and R. A. Polanczyk, *J. Agric. Food Chem.*, 2021, **69**, 4564–4577.
11 G. Kowalska, J. Rosicka-Kaczmarek, K. Miśkiewicz, M. Zakłos-Szyda, S. Rohn, C. Kanzler, M. Wiktorska and J. Niewiarowska, *Nutrients*, 2022, **14**, 2529.
12 J. S. Ribeiro and C. M. Veloso, *Food Hydrocolloids*, 2021, **112**, 106374.
13 Z. Fang, X.-R. Cao, Y.-L. Yu and M. Li, *Colloids Surf., A*, 2019, **570**, 282–292.
14 B. Zhou, W. Kang, H. Jiang, H. Yang, Z. Li, Z. Lv, Z. Xu, C. Ning, H. Wang and S. Xie, *J. Pet. Sci. Eng.*, 2022, **219**, 111122.
15 W. Li, L. Zhang, X. Ge, B. Xu, W. Zhang, L. Qu, C.-H. Choi, J. Xu, A. Zhang, H. Lee and D. A. Weitz, *Chem. Soc. Rev.*, 2018, **47**, 5646–5683.
16 A. Gonzalez Gomez and Z. Hosseinidoust, *ACS Infect. Dis.*, 2020, **6**, 896–908.
17 P. Velmurugan, V. Ganeshan, N. F. Nishter and R. R. Jonnalagadda, *Surf. Interfaces*, 2017, **9**, 124–132.
18 M. Mamusa, C. Sofroniou, C. Resta, S. Murgia, E. Fratini, J. Smets and P. Baglioni, *ACS Appl. Mater. Interfaces*, 2020, **12**, 28808–28818.
19 S. Natour and R. Abu-Reziq, *RSC Adv.*, 2014, **4**, 48299–48309.
20 H. O. Otor, J. B. Steiner, C. García-Sancho and A. C. Alba-Rubio, *ACS Catal.*, 2020, **10**, 7630–7656.
21 Z. Liu, F. Fontana, A. Python, J. T. Hirvonen and H. A. Santos, *Small*, 2019, **16**, 1904673.
22 Q. Zhang, N. F. Inagaki, H. Yoshida, M. Kamihira, Y. Sakai and T. Ito, *J. Membr. Sci.*, 2024, **689**, 122119.

23 N. Teo, C. Jin, A. Kulkarni and S. C. Jana, *J. Colloid Interface Sci.*, 2020, **561**, 772–781.
24 Y. Zhao, Z. Xie, H. Gu, L. Jin, X. Zhao, B. Wang and Z. Gu, *NPG Asia Mater.*, 2012, **4**, e25–e25.
25 X. Huang and B. Voit, *Polym. Chem.*, 2013, **4**, 435–443.
26 N. K. Preman, R. R. Barki, A. Vijayan, S. G. Sanjeeva and R. P. Johnson, *Eur. J. Pharm. Biopharm.*, 2020, **157**, 121–153.
27 G. G. Abdo, M. M. Zagho and A. Khalil, *Emergent Mater.*, 2020, **3**, 407–425.
28 A. Rezaei, F. Rafieian, S. Akbari-Alavijeh, M. S. Kharazmi and S. M. Jafari, *Adv. Colloid Interface Sci.*, 2022, **307**, 102728.
29 D. Wandera, S. R. Wickramasinghe and S. M. Husson, *J. Membr. Sci.*, 2010, **357**, 6–35.
30 X. Ju and L. Chu, *R. Soc. Chem*, 2019, 255–296.
31 K. Thananukul, C. Kaewsaneha, P. Opaprakasit, N. Lebaz, A. Errachid and A. Elaissari, *Adv. Drug Delivery Rev.*, 2021, **174**, 425–446.
32 P. Zhu and L. Wang, *Lab Chip*, 2016, **17**, 34–75.
33 J. Guerrero, Y. Chang, A. A. Fragkopoulos and A. Fernandez-Nieves, *Small*, 2019, **16**, e1904344.
34 A. Kamnerdsook, E. Juntasaro, N. Khemthongcharoen, M. Chanasakulniyom, W. Sripumkhai, P. Pattamang, C. Promptmas, N. Atthi and W. Jeamsaksiri, *RSC Adv.*, 2021, **11**, 35653–35662.
35 F. Fontana, M. P. A. Ferreira, A. Correia, J. Hirvonen and H. A. Santos, *J. Drug Delivery Sci. Technol.*, 2016, **34**, 76–87.
36 D. R. Link, S. L. Anna, D. A. Weitz and H. A. Stone, *Phys. Rev. Lett.*, 2004, **92**, 054503.
37 T. M. Tran, F. Lan, C. S. Thompson and A. R. Abate, *J. Phys. D: Appl. Phys.*, 2013, **46**, 114004.
38 A. S. Utada, A. Fernandez-Nieves, H. A. Stone and D. A. Weitz, *Phys. Rev. Lett.*, 2007, **99**, 094502.
39 W.-A. C. Bauer, M. Fischlechner, C. Abell and W. T. S. Huck, *Lab Chip*, 2010, **10**, 1814–1819.
40 D. Li, X. Li, C. Chen, Z. Zheng and H. Chang, *Sens. Actuators, B*, 2018, **255**, 1048–1056.
41 A. M. Nightingale, S. H. Krishnadasan, D. Berhanu, X. Niu, C. Drury, R. McIntyre, E. Valsami-Jones and J. C. deMello, *Lab Chip*, 2011, **11**, 1221–1227.
42 P. N. Nge, C. I. Rogers and A. T. Woolley, *Chem. Rev.*, 2013, **113**, 2550–2583.
43 V. Narayanamurthy, Z. E. Jeroish, K. S. Bhuvaneshwari, P. Bayat, R. Premkumar, F. Samsuri and M. M. Yusoff, *RSC Adv.*, 2020, **10**, 11652–11680.
44 A. Olanrewaju, M. Beaugrand, M. Yafia and D. Juncker, *Lab Chip*, 2018, **18**, 2323–2347.
45 W. J. Duncanson, T. Lin, A. R. Abate, S. Seiffert, R. K. Shah and D. A. Weitz, *Lab Chip*, 2012, **12**, 2135–2145.
46 M. P. Wolf, G. B. Salieb-Beugelaar and P. Hunziker, *Prog. Polym. Sci.*, 2018, **83**, 97–134.
47 A. Shakeri, S. Khan and T. F. Didar, *Lab Chip*, 2021, **21**, 3053–3075.
48 R. K. Shah, H. C. Shum, A. C. Rowat, D. Lee, J. J. Agresti, A. S. Utada, L.-Y. Chu, J.-W. Kim, A. Fernandez-Nieves, C. J. Martinez and D. A. Weitz, *Mater. Today*, 2008, **11**, 18–27.
49 Q. Xu and J. Jiang, *ACS Appl. Polym. Mater.*, 2020, **2**, 3576–3586.
50 J. Zhou, D. A. Khodakov, A. V. Ellis and N. H. Voelcker, *Electrophoresis*, 2012, **33**, 89–104.
51 S. C. Kim, D. J. Sukovich and A. R. Abate, *Lab Chip*, 2015, **15**, 3163–3169.
52 N. Bodin-Thomazo, F. Malloggi and P. Guenoun, *RSC Adv.*, 2017, **7**, 46514–46519.
53 T. M. Tran, F. Lan, C. S. Thompson and A. R. Abate, *J. Phys. D: Appl. Phys.*, 2013, **46**, 114004.
54 L. Montazeri, S. Bonakdar, M. Taghipour, P. Renaud and H. Baharvand, *Lab Chip*, 2016, **16**, 2596–2600.
55 A. R. Abate, D. Lee, T. Do, C. Holtze and D. A. Weitz, *Lab Chip*, 2008, **8**, 516–518.
56 S. Hwang, C. H. Choi and C. S. Lee, *Macromol. Res.*, 2012, **20**, 422–428.
57 D.-K. Lee, S. Y. Choi, M. S. Park and Y. H. Cho, *Appl. Phys. A: Mater. Sci. Process.*, 2018, **124**, 192.
58 D. R. Link, S. L. Anna, D. A. Weitz and H. A. Stone, *Phys. Rev. Lett.*, 2004, **92**, 054503.
59 Z. Bai, B. Wang, H. Chen and M. Wang, *Sens. Actuators, B*, 2015, **215**, 330–336.
60 N. Leister, G. T. Vladisavljević and H. P. Karbstein, *J. Colloid Interface Sci.*, 2022, **611**, 451–461.
61 Z. Chen, Z. Lv, Z. Zhang, D. A. Weitz, H. Zhang, Y. Zhang and W. Cui, *Exploration*, 2021, **1**, 20210036.
62 A. R. Abate, A. Poitzsch, Y. Hwang, J. Lee, J. Czerwinska and D. A. Weitz, *Phys. Rev. E*, 2009, **80**, 026310.
63 J. K. Nunes, S. S. H. Tsai, J. Wan and H. A. Stone, *J. Phys. D: Appl. Phys.*, 2013, **46**, 114002.
64 S. Seiffert, J. Thiele, A. R. Abate and D. A. Weitz, *J. Am. Chem. Soc.*, 2010, **132**, 6606–6609.
65 M. Seo, C. Paquet, Z. Nie, S. Xu and E. Kumacheva, *Soft Matter*, 2007, **3**, 986–992.
66 C. Mou, W. Wang, Z. Li, X. Ju, R. Xie, N. Deng, J. Wei, Z. Liu and L. Chu, *Adv. Sci.*, 2018, **5**, 1700960.
67 Z. Sun, C. Yang, M. Eggersdorfer, J. Cui, Y. Li, M. Hai, D. Chen and D. A. Weitz, *Chin. Chem. Lett.*, 2020, **31**, 249–252.
68 L. Zhang, L.-H. Cai, P. S. Lienemann, T. Rossow, I. Polenz, Q. Vallmajo-Martin, M. Ehrbar, H. Na, D. J. Mooney and D. A. Weitz, *Angew. Chem., Int. Ed.*, 2016, **55**, 13470–13474.
69 L. Shang, Y. Cheng, J. Wang, H. Ding, F. Rong, Y. Zhao and Z. Gu, *Lab Chip*, 2014, **14**, 3489–3493.
70 H. Zhang, L. Zhang, C. An, Y. Zhang, F. Shao, Y. Gao, Y. Zhang, H. Li, Y. Zhang, C. Ren, K. Sun, W. He, F. Cheng, H. Wang and D. A. Weitz, *Biofabrication*, 2022, **14**, 035015.
71 T. Femmer, A. Jans, R. Eswein, N. Anwar, M. Moeller, M. Wessling and A. J. C. Kuehne, *ACS Appl. Mater. Interfaces*, 2015, **7**, 12635–12638.
72 D. M. Headen, J. R. García and A. J. García, *Microsyst. Nanoeng.*, 2018, **4**, 1–9.
73 S. Shin, S. Cho, R. Song, H. Kim and J. Lee, *Chem. Eng. J.*, 2023, **471**, 144734.
74 J. H. Xu, S. W. Li, J. Tan, Y. J. Wang and G. S. Luo, *Langmuir*, 2006, **22**, 7943–7946.

75 A. S. Utada, E. Lorenceau, D. R. Link, P. D. Kaplan, H. A. Stone and D. A. Weitz, *Science*, 2005, **308**, 537–541.
76 W. Ma, C. Mou, S. Chen, Y. Li and H. Deng, *Polymer*, 2022, **14**, 1165.
77 G. Chen, C. H. Niu, M.-Y. Zhou, X.-J. Ju, R. Xie and L.-Y. Chu, *J. Colloid Interface Sci.*, 2010, **343**, 168–175.
78 M.-J. Zhang, W. Wang, R. Xie, X.-J. Ju, L. Liu, Y.-Y. Gu and L.-Y. Chu, *Soft Matter*, 2013, **9**, 4150–4159.
79 P. B. Umbanhowar, V. Prasad and D. A. Weitz, *Langmuir*, 1999, **16**, 347–351.
80 C.-L. Mou, Q.-Z. Deng, J.-X. Hu, L.-Y. Wang, H.-B. Deng, G. Xiao and Y. Zhan, *J. Colloid Interface Sci.*, 2020, **569**, 307–319.
81 Q. Xu, M. Hashimoto, T. T. Dang, T. Hoare, D. S. Kohane, G. M. Whitesides, R. Langer and D. G. Anderson, *Small*, 2009, **5**, 1575–1581.
82 S. Takeuchi, P. Garstecki, D. B. Weibel and G. M. Whitesides, *Adv. Mater.*, 2005, **17**, 1067–1072.
83 C. Choi, H. Lee, A. Abbaspourrad, J. H. Kim, J. Fan, M. Caggioni, C. Wesner, T. Zhu and D. A. Weitz, *Adv. Mater.*, 2016, **28**, 3340–3344.
84 Y. Oh and S. Kim, *J. Polym. Sci.*, 2021, **60**, 1700–1709.
85 B. Kim, S. Lee and S.-H. Kim, *Adv. Mater. Interfaces*, 2018, **5**, 1701472.
86 X.-C. Song, Y.-L. Yu, G.-Y. Yang, A.-L. Jiang, Y. Ruan and S. Fan, *Colloids Surf., B*, 2022, **216**, 112560.
87 S. Lee, B. Che, M. Tai, W. Li and S.-H. Kim, *Adv. Funct. Mater.*, 2021, **31**, 2105477.
88 S.-H. Kim and D. A. Weitz, *Angew. Chem.*, 2011, **123**, 8890–8893.
89 M. Brzeziński, M. Socka and B. Kost, *Polym. Int.*, 2019, **68**, 997–1014.
90 L. Liu, N. Xiang, Z. Ni, X. Huang, J. Zheng, Y. Wang and X. Zhang, *BioTechniques*, 2020, **68**, 114–116.
91 A. C. Daly, L. Riley, T. Segura and J. A. Burdick, *Nat. Rev. Mater.*, 2019, **5**, 20–43.
92 Q.-W. Cai, X.-J. Ju, S.-Y. Zhang, Z.-H. Chen, J.-Q. Hu, L.-P. Zhang, R. Xie, W. Wang, Z. Liu and L.-Y. Chu, *ACS Appl. Mater. Interfaces*, 2019, **11**, 46241–46250.
93 T. Nisisako, T. Torii, T. Takahashi and Y. Takizawa, *Adv. Mater.*, 2006, **18**, 1152–1156.
94 N. Prasad, J. Perumal, C.-H. Choi, C.-S. Lee and D.-P. Kim, *Adv. Funct. Mater.*, 2009, **19**, 1656–1662.
95 M. H. Lee, K. C. Hribar, T. Brugarolas, N. P. Kamat, J. A. Burdick and D. Lee, *Adv. Funct. Mater.*, 2011, **22**, 131–138.
96 Z. Feng, B. Zhou, X. Su, T. Wang, S. Guo, H. Yang and X. Sun, *Mater. Des.*, 2023, **225**, 111516.
97 A. D. Bick, J. W. Khor, Y. Gai and S. K. Y. Tang, *Proc. Natl. Acad. Sci. U. S. A.*, 2021, **118**, e2017822118.
98 Y. Gao, C.-X. Zhao and F. Sainsbury, *J. Colloid Interface Sci.*, 2021, **584**, 528–538.
99 M.-J. Zhang, P. Zhang, L.-D. Qiu, T. Chen, W. Wang and L.-Y. Chu, *Biomicrofluidics*, 2020, **14**, 061501.
100 W. Wang, T. Luo, X.-J. Ju, R. Xie, L. Liu and L.-Y. Chu, *Int. J. Nonlinear Sci. Numer. Simul.*, 2012, **13**, 325–332.
101 M. Weiss, J. P. Frohnmayer, L. T. Benk, B. Haller, J.-W. Janiesch, T. Heitkamp, M. Börsch, R. B. Lira, R. Dimova, R. Lipowsky, E. Bodenschatz, J.-C. Baret, T. Vidakovic-Koch, K. Sundmacher, I. Platzman and J. P. Spatz, *Nat. Mater.*, 2018, **17**, 89–96.
102 Z.-M. Liu, Y. Yang, Y. Du and Y. Pang, *Chin. J. Anal. Chem.*, 2017, **45**, 282–296.
103 Q. Xu, M. Hashimoto, T. T. Dang, T. Hoare, D. S. Kohane, G. M. Whitesides, R. Langer and D. G. Anderson, *Small*, 2009, **5**, 1575–1581.
104 H. Pei, A. Abbaspourrad, W. Zhang, Z. Wu and D. A. Weitz, *Macromol. Mater. Eng.*, 2019, **304**, 1900156.
105 X.-T. Mu, X.-J. Ju, L. Zhang, X.-B. Huang, Y. Faraj, Z. Liu, W. Wang, R. Xie, Y. Deng and L.-Y. Chu, *J. Membr. Sci.*, 2019, **590**, 117275.
106 J. Li, L. Jia, Y. Chen, L. Li, S. Mo, J. Wang and C. Wang, *Appl. Therm. Eng.*, 2019, **162**, 114278.
107 H. A. Son, S. K. Choi, E. S. Jeong, B. Kim, H. T. Kim, W. M. Sung and J. W. Kim, *Langmuir*, 2016, **32**, 8909–8915.
108 Z. Luo, G. Zhao, F. Panhwar, M. F. Akbar and Z. Shu, *J. Drug Delivery Sci. Technol.*, 2017, **39**, 379–384.
109 C. Siltanen, M. Diakatou, J. Lowen, A. Haque, A. Rahimian, G. Stybayeva and A. Revzin, *Acta Biomater.*, 2017, **50**, 428–436.
110 X. Wang, M. Zhu, K. Wang, S. He, X. Shi, B. Yuan, B. Dong and Z. Wang, *J. Drug Delivery Sci. Technol.*, 2022, **72**, 103361.
111 E. Loiseau, P. A. Rühs, A. Hauser, F. Niedermair, G. Albrecht and A. R. Studart, *Langmuir*, 2018, **34**, 205–212.
112 H. Lee, C.-H. Choi, A. Abbaspourrad, C. Wesner, M. Caggioni, T. Zhu and D. A. Weitz, *ACS Appl. Mater. Interfaces*, 2016, **8**, 4007–4013.
113 H. Kim, S. Jo, F. Meng, Y. Guo, H. Thérien-Aubin, R. Golestanian, K. Landfester and E. Bodenschatz, *Adv. Funct. Mater.*, 2020, **30**, 2006019.
114 B. J. Sun, H. C. Shum, C. Holtze and D. A. Weitz, *ACS Appl. Mater. Interfaces*, 2010, **2**, 3411–3416.
115 S. S. Lee, J. Park, Y. Seo and S.-H. Kim, *ACS Appl. Mater. Interfaces*, 2017, **9**, 17178–17185.
116 H.-S. Jeong, E. Kim, C. Nam, Y. Choi, Y.-J. Lee, D. A. Weitz, H. Lee and C.-H. Choi, *Adv. Funct. Mater.*, 2021, **31**, 2009553.
117 L. Liu, W. Wang, X.-J. Ju, R. Xie and L.-Y. Chu, *Soft Matter*, 2010, **6**, 3759–3763.
118 F. He, M. Zhang, W. Wang, Q. Cai, Y. Su, Z. Liu, Y. Faraj, X. Ju, R. Xie and L. Chu, *Adv. Mater. Technol.*, 2019, **4**, 1800687.
119 M. Steinacher, A. Cont, H. Du, A. Persat and E. Amstad, *ACS Appl. Mater. Interfaces*, 2021, **13**, 15601–15609.
120 K. Zhang, Y. Ren, T. Jiang and H. Jiang, *Anal. Chim. Acta*, 2021, **1182**, 338955.
121 C.-H. Choi, S. Hwang, J.-M. Jeong, S.-M. Kang, J. Kim and C.-S. Lee, *Biomed. Eng. Lett.*, 2012, **2**, 95–99.
122 T. Kamperman, V. D. Trikalitis, M. Karperien, C. W. Visser and J. Leijten, *ACS Appl. Mater. Interfaces*, 2018, **10**, 23433–23438.

123 Y. Shen, L. Yuan, G. Wu, W. Yuan, Z. Cheng, J. Yan, J. Zhang, Y. Tao and Z. Yu, *ACS Appl. Mater. Interfaces*, 2023, **15**, 591–598.
124 Q.-W. Cai, D.-W. Pan, X.-J. Ju, C. Chen, L.-P. Zhang, S.-H. Yang, R. Xie, W. Wang, Z. Liu and L.-Y. Chu, *ACS Appl. Polym. Mater.*, 2023, **5**, 5525–5536.
125 B. Haney, J. G. Werner, D. A. Weitz and S. Ramakrishnan, *Soft Matter*, 2020, **16**, 3613–3620.
126 L. Weidenbacher, A. Abrishamkar and M. Rottmar, *Acta Biomater.*, 2017, **64**, 137–147.
127 Y. Wang, J. Yuan, S. Dong and J. Hao, *Langmuir*, 2022, **38**, 4713–4721.
128 H. Shum, J. Varnell and D. A. Weitz, *Biomicrofluidics*, 2012, **6**, 12808–128089.
129 R. A. de Freitas, T. Nicolai, C. Chassenieux and L. Benyahia, *Langmuir*, 2016, **32**, 1227–1232.
130 J. Zhang, J. Hwang, M. Antonietti and B. V. K. J. Schmidt, *Biomacromolecules*, 2018, **20**, 204–211.
131 D. Liu, H. Zhang, B. Herranz-Blanco, E. Mäkilä, V. Lehto, J. Salonen, J. Hirvonen and H. A. Santos, *Small*, 2014, **10**, 2029–2038.
132 Y. Du, L. Mo, X. Wang, H. Wang, X. Ge and T. Qiu, *Microfluid. Nanofluid.*, 2020, **24**, 42.
133 W. Zhang, L. Qu, H. Pei, Z. Qin, J. Didier, Z. Wu, F. Bobe, D. E. Ingber and D. A. Weitz, *Small*, 2019, **15**, 1903087.
134 Z. Wu, J. G. Werner and D. A. Weitz, *ACS Macro Lett.*, 2021, **10**, 116–121.
135 E. Loiseau, F. Niedermair, G. Albrecht, M. Frey, A. Hauser, P. A. Rühs and A. R. Studart, *Langmuir*, 2017, **33**, 2402–2410.
136 H. Seo and H. Lee, *Nat. Commun.*, 2022, **13**, 5179.
137 R. Luo, S. Pashapour, O. Staufer, I. Platzman and J. P. Spatz, *Adv. Funct. Mater.*, 2020, **30**, 1908855.
138 R. L. Siegelman, E. J. Kim and J. R. Long, *Nat. Mater.*, 2021, **20**, 1060–1072.
139 G. Michielin and S. J. Maerkl, *Sci. Rep.*, 2022, **12**, 21391.
140 X. Liu, Y. Yu, D. Liu, J. Li, J. Sun, Q. Wei, Y. Zhao, S. J. Pandol and L. Li, *NPG Asia Mater.*, 2022, **14**, 1–10.
141 W. J. Duncanson, M. Zieringer, O. Wagner, J. N. Wilking, A. Abbaspourrad, R. Haag and D. A. Weitz, *Soft Matter*, 2012, **8**, 10636–10640.
142 X. Xie, W. Zhang, A. Abbaspourrad, J. Ahn, A. Bader, S. Bose, A. Vegas, J. Lin, J. Tao, T. Hang, H. Lee, N. Iverson, G. Bisker, L. Li, M. S. Strano, D. A. Weitz and D. G. Anderson, *Nano Lett.*, 2017, **17**, 2015–2020.
143 T. Bollhorst, K. Rezwan and M. Maas, *Chem. Soc. Rev.*, 2017, **46**, 2091–2126.
144 A. Laromaine, T. Tronser, I. Pini, S. Parets, P. A. Levkin and A. Roig, *Soft Matter*, 2018, **14**, 3955–3962.
145 D. Lee and D. A. Weitz, *Adv. Mater.*, 2008, **20**, 3498–3503.
146 J. S. Sander and A. R. Studart, *Langmuir*, 2011, **27**, 3301–3307.
147 A. D. Dinsmore, M. F. Hsu, M. G. Nikolaides, M. Marquez, A. R. Bausch and D. A. Weitz, *Science*, 2002, **298**, 1006–1009.
148 M. D. Rintoul and S. Torquato, *Phys. Rev. E*, 1998, **58**, 532–537.
149 D. A. Olson, L. Chen and M. A. Hillmyer, *Chem. Mater.*, 2008, **20**, 869–890.
150 B. Kim, T. Y. Lee, A. Abbaspourrad and S.-H. Kim, *Chem. Mater.*, 2014, **26**, 7166–7171.
151 B. Kim, T. Y. Jeon, Y.-K. Oh and S.-H. Kim, *Langmuir*, 2015, **31**, 6027–6034.
152 L. Chen, Y. Xiao, Z. Zhang, C.-X. Zhao, B. Guo, F. Ye and D. Chen, *Front. Chem. Sci. Eng.*, 2022, **16**, 1643–1650.
153 R. T. Rosenberg and N. R. Dan, *J. Colloid Interface Sci.*, 2010, **349**, 498–504.
154 S.-H. Kim, H. C. Shum, J. W. Kim, J.-C. Cho and D. A. Weitz, *J. Am. Chem. Soc.*, 2011, **133**, 15165–15171.
155 F. Meng, Z. Zhong and J. Feijen, *Biomacromolecules*, 2009, **10**, 197–209.
156 I. Meerovich and A. K. Dash, in *Materials for Biomedical Engineering*, ed. A.-M. Holban and A. M. Grumezescu, Elsevier, 2019, pp. 269–309.
157 E. Amstad, S.-H. Kim and D. A. Weitz, *Angew. Chem., Int. Ed.*, 2012, **51**, 12499–12503.
158 X. Wang, J. Hu and S. Liu, *Acc. Chem. Res.*, 2022, **55**, 3404–3416.
159 Z. Gao, X. Cui and J. Cui, *Supramolecular Materials*, 2022, **1**, 100015.
160 W. Xu, P. A. Ledin, Z. Iatridi, C. Tsitsilianis and V. V. Tsukruk, *Angew. Chem., Int. Ed.*, 2016, **55**, 4908–4913.
161 Y. Zhao, H. C. Shum, H. Chen, L. L. A. Adams, Z. Gu and D. A. Weitz, *J. Am. Chem. Soc.*, 2011, **133**, 8790–8793.
162 N.-N. Deng, M. Yelleswarapu and W. T. S. Huck, *J. Am. Chem. Soc.*, 2016, **138**, 7584–7591.
163 J.-O. Chu, Y. Choi, D.-W. Kim, H.-S. Jeong, J. P. Park, D. A. Weitz, S.-J. Lee, H. Lee and C.-H. Choi, *ACS Appl. Mater. Interfaces*, 2022, **14**, 2597–2604.
164 S. Lee, T. Y. Lee, E. Amstad and S. Kim, *Adv. Mater. Technol.*, 2018, **3**, 1800006.
165 E. A. Sykes, J. Chen, G. Zheng and W. C. W. Chan, *ACS Nano*, 2014, **8**, 5696–5706.
166 J. W. Hickey, J. L. Santos, J.-M. Williford and H.-Q. Mao, *J. Controlled Release*, 2015, **219**, 536–547.
167 Z. Zhao, A. Ukidve, V. Krishnan and S. Mitragotri, *Adv. Drug Delivery Rev.*, 2019, **143**, 3–21.
168 D. A. Canelas, K. P. Herlihy and J. M. DeSimone, *Wiley Interdiscip. Rev.: Nanomed. Nanobiotechnol.*, 2009, **1**, 391–404.
169 Z. Dai, M. Yu, X. Yi, Z. Wu, F. Tian, Y. Miao, W. Song, S. He, E. Ahmad, S. Guo, C. Zhu, X. Zhang, Y. Li, X. Shi, R. Wang and Y. Gan, *ACS Nano*, 2019, **13**, 7676–7689.
170 M. T. Manzari, Y. Shamay, H. Kiguchi, N. Rosen, M. Scaltriti and D. A. Heller, *Nat. Rev. Mater.*, 2021, **6**, 351–370.
171 K. Maruyama, *Adv. Drug Delivery Rev.*, 2011, **63**, 161–169.
172 C. Kuroda, C. Mochizuki, J. Nakamura and M. Nakamura, *OpenNano*, 2023, **9**, 100114.
173 Y.-N. Zhang, J. Lazarovits, W. Poon, B. Ouyang, L. N. M. Nguyen, B. R. Kingston and W. C. W. Chan, *Nano Lett.*, 2019, **19**, 7226–7235.

174 L. Qin, F. Zhang, X. Lu, X. Wei, J. Wang, X. Fang, D. Si, Y. Wang, C. Zhang, R. Yang, C. Liu and W. Liang, *J. Controlled Release*, 2013, **171**, 133–142.
175 L. Mei, J. Rao, Y. Liu, M. Li, Z. Zhang and Q. He, *J. Controlled Release*, 2018, **292**, 67–77.
176 Q. Meng, S. Zhong, L. Xu, J. Wang, Z. Zhang, Y. Gao and X. Cui, *Carbohydr. Polym.*, 2022, **279**, 119013.
177 S. Wilhelm, A. J. Tavares, Q. Dai, S. Ohta, J. Audet, H. F. Dvorak and W. C. W. Chan, *Nat. Rev. Mater.*, 2016, **1**, 16014.
178 E. A. Sykes, Q. Dai, C. D. Sarsons, J. Chen, J. V. Rocheleau, D. M. Hwang, G. Zheng, D. T. Cramb, K. D. Rinker and W. C. W. Chan, *Proc. Natl. Acad. Sci. U. S. A.*, 2016, **113**, E1142–E1151.
179 C. M. Dawidczyk, L. M. Russell and P. C. Searson, *Front. Chem.*, 2014, **2**, 69.
180 Y. Sun and E. Davis, *Nanomaterials*, 2021, **11**, 746.
181 Q. Meng, S. Zhong, L. Xu, J. Wang, Z. Zhang, Y. Gao and X. Cui, *Carbohydr. Polym.*, 2022, **279**, 119013.
182 F. Perche, S. Biswas, T. Wang, L. Zhu and V. P. Torchilin, *Angew. Chem.*, 2014, **126**, 3430–3434.
183 H.-J. Li, J.-Z. Du, J. Liu, X.-J. Du, S. Shen, Y.-H. Zhu, X. Wang, X. Ye, S. Nie and J. Wang, *ACS Nano*, 2016, **10**, 6753–6761.
184 C. Arya, H. Oh and S. R. Raghavan, *ACS Appl. Mater. Interfaces*, 2016, **8**, 29688–29695.
185 B. K. Kaang, S. Lee, J. Piao, H. J. Cho and D.-P. Kim, *Lab Chip*, 2023, **23**, 2829–2837.
186 M. Xie, W. Zhang, C. Fan, C. Wu, Q. Feng, J. Wu, Y. Li, R. Gao, Z. Li, Q. Wang, Y. Cheng and B. He, *Adv. Mater.*, 2020, **32**, 2000366.
187 Z. Li, E. Ye, David, R. Lakshminarayanan and X. J. Loh, *Small*, 2016, **12**, 4782–4806.
188 J. Wei, X.-J. Ju, X.-Y. Zou, R. Xie, W. Wang, Y.-M. Liu and L.-Y. Chu, *Adv. Funct. Mater.*, 2014, **24**, 3312–3323.
189 M. Navi, J. Kieda and S. S. H. Tsai, *Lab Chip*, 2020, **20**, 2851–2860.
190 Y.-M. Liu, W. Wu, X.-J. Ju, W. Wang, R. Xie, C.-L. Mou, W.-C. Zheng, Z. Liu and L.-Y. Chu, *RSC Adv.*, 2014, **4**, 46568–46575.
191 X. Kong, P. Gao, J. Wang, Y. Fang and K. C. Hwang, *J. Hematol. Oncol.*, 2023, **16**, 74.
192 Z. Wang, Z. Xu, B. Zhu, Y. Zhang, J. Lin, Y. Wu and D. Wu, *Nanotechnology*, 2022, **33**, 152001.
193 Z. Liu, W. Wang, R. Xie, X.-J. Ju and L.-Y. Chu, *Chem. Soc. Rev.*, 2016, **45**, 460–475.
194 F. B. Arslan, K. Ozturk and S. Calis, *Int. J. Pharm.*, 2021, **596**, 120268.
195 Z. Han, W. Lv, Y. Li, J. Chang, W. Zhang, C. Liu and J. Sun, *ACS Appl. Bio Mater.*, 2020, **3**, 2666–2673.
196 G. Sanità, P. Armanetti, B. Silvestri, B. Carrese, G. Calì, G. Pota, A. Pezzella, M. d'Ischia, G. Luciani, L. Menichetti and A. Lamberti, *Front. Bioeng. Biotechnol.*, 2020, **8**, 765.
197 Y. Li, G. Yang, L. Gerstweiler, S. H. Thang and C.-X. Zhao, *Adv. Funct. Mater.*, 2023, **33**, 2210387.
198 L. Ramzy, A. A. Metwally, M. Nasr and G. A. S. Awad, *Sci. Rep.*, 2020, **10**, 10987.
199 D. E. Large, J. R. Soucy, J. Hebert and D. T. Auguste, *Adv. Ther.*, 2018, **2**, 1800091.
200 Y. Bae, W.-D. Jang, N. Nishiyama, S. Fukushima and K. Kataoka, *Mol. BioSyst.*, 2005, **1**, 242.
201 S. Rai, R. Paliwal, B. Vaidya, K. Khatri, A. K. Goyal, P. N. Gupta and S. P. Vyas, *J. Drug Targeting*, 2008, **16**, 455–463.
202 Y. Zhang, Y. Wang, X. Li, D. Nie, C. Liu and Y. Gan, *J. Controlled Release*, 2022, **352**, 813–832.
203 P. Mi, H. Cabral and K. Kataoka, *Adv. Mater.*, 2020, **32**, 1902604.
204 G. Sanità, P. Armanetti, B. Silvestri, B. Carrese, G. Calì, G. Pota, A. Pezzella, M. d'Ischia, G. Luciani, L. Menichetti and A. Lamberti, *Front. Bioeng. Biotechnol.*, 2020, **8**, 354–365.
205 N. AlSawaftah, W. G. Pitt and G. A. Husseini, *ACS Pharmacol. Transl. Sci.*, 2021, **4**, 1028–1049.
206 N. Khan, Ruchika, R. K. Dhritlahre and A. Saneja, *Drug Discovery Today*, 2022, **27**(8), 2288–2299.
207 S. Sun, H. Zou, L. Li, Q. Liu, N. Ding, L. Zeng, H. Li and S. Mao, *Int. J. Pharm.*, 2019, **568**, 118518.
208 J. Tang, C. B. Howard, S. M. Mahler, K. J. Thurecht, L. Huang and Z. P. Xu, *Nanoscale*, 2018, **10**, 4258–4266.
209 R. Ran, H. Wang, Y. Liu, Y. Hui, Q. Sun, A. Seth, D. Wibowo, D. Chen and C.-X. Zhao, *Eur. J. Pharm. Biopharm.*, 2018, **130**, 1–10.
210 J. Chen, J. Ding, W. Xu, T. Sun, H. Xiao, X. Zhuang and X. Chen, *Nano Lett.*, 2017, **17**, 4526–4533.
211 T. Yang, A. Wang, D. Nie, W. Fan, X. Jiang, M. Yu, S. Guo, C. Zhu, G. Wei and Y. Gan, *Nat. Commun.*, 2022, **13**, 6649.
212 Q. Xia, H. Ding and Y. Ma, *Nanoscale*, 2017, **9**, 8982–8989.
213 S. Maslanka Figueroa, D. Fleischmann and A. Goepferich, *J. Controlled Release*, 2021, **329**, 552–569.
214 M. K. Prajapati, R. Pai and P. Vavia, *J. Drug Delivery Sci. Technol.*, 2021, **66**, 102809.
215 J. Shang and X. Gao, *Chem. Soc. Rev.*, 2014, **43**, 7267–7278.
216 A. M. Alkilany, L. Zhu, H. Weller, A. Mews, W. J. Parak, M. Barz and N. Feliu, *Adv. Drug Delivery Rev.*, 2019, **143**, 22–36.
217 Y. Liu, Y. Hui, R. Ran, G.-Z. Yang, D. Wibowo, H.-F. Wang, A. P. J. Middelberg and C.-X. Zhao, *Adv. Healthcare Mater.*, 2018, **7**, 1800106.
218 S. Mura, J. Nicolas and P. Couvreur, *Nat. Mater.*, 2013, **12**, 991–1003.
219 Q. Xia, T. Zhu, Z. Jiang, H. Ding and Y. Ma, *Nanoscale*, 2020, **12**, 7804–7813.
220 Y. Liu, R. Dai, Q. Wei, W. Li, G. Zhu, H. Chi, Z. Guo, L. Wang, C. Cui, J. Xu and K. Ma, *ACS Appl. Mater. Interfaces*, 2019, **11**, 44582–44592.
221 W. Liu, Q. Wu, W. Wang, X. Xu, C. Yang and Y. Song, *TrAC, Trends Anal. Chem.*, 2022, **157**, 116827.
222 U. Dharmasiri, S. K. Njoroge, M. A. Witek, M. G. Adebiyi, J. W. Kamande, M. L. Hupert, F. Barany and S. A. Soper, *Anal. Chem.*, 2011, **83**, 2301–2309.

223 H. Wijerathne, M. A. Witek, J. M. Jackson, V. Brown, M. L. Hupert, K. Herrera, C. Kramer, A. E. Davidow, Y. Li, A. E. Baird, M. C. Murphy and S. A. Soper, *Commun. Biol.*, 2020, **3**, 613.
224 Y. Gou, Z. Chen, C. Sun, P. Wang, Z. You, Y. Yalikun, Y. Tanaka and D. Ren, *Nanoscale*, 2021, **13**, 17765–17774.
225 P. Zhang, X. Zhou, M. He, Y. Shang, A. L. Tetlow, A. K. Godwin and Y. Zeng, *Nat. Biomed. Eng.*, 2019, **3**, 438–451.
226 M. G. Ahmed, M. F. Abate, Y. Song, Z. Zhu, F. Yan, Y. Xu, X. Wang, Q. Li and C. Yang, *Angew. Chem., Int. Ed.*, 2017, **56**, 10681–10685.
227 S. L. Stott, C.-H. Hsu, D. I. Tsukrov, M. Yu, D. T. Miyamoto, B. A. Waltman, S. M. Rothenberg, A. M. Shah, M. E. Smas, G. K. Korir, F. P. Floyd, A. J. Gilman, J. B. Lord, D. Winokur, S. Springer, D. Irimia, S. Nagrath, L. V. Sequist, R. J. Lee, K. J. Isselbacher, S. Maheswaran, D. A. Haber and M. Toner, *Proc. Natl. Acad. Sci. U. S. A.*, 2010, **107**, 18392–18397.
228 L. Wu, H. Ding, X. Qu, X. Shi, J. Yang, M. Huang, J. Zhang, H. Zhang, J. Song, L. Zhu, Y. Song, Y. Ma and C. Yang, *J. Am. Chem. Soc.*, 2020, **142**, 4800–4806.
229 J. Zhang, B. Lin, L. Wu, M. Huang, X. Li, H. Zhang, J. Song, W. Wang, G. Zhao, Y. Song and C. Yang, *Angew. Chem., Int. Ed.*, 2020, **59**, 14115–14119.
230 E. Assadpour and S. M. Jafari, *Release and Bioavailability of Nanoencapsulated Food Ingredients*, 2020, vol. 5, pp. 1–24.
231 S. Boostani and S. M. Jafari, *Release and Bioavailability of Nanoencapsulated Food Ingredients*, 2020, vol. 5, pp. 27–78.
232 A. M. DiLauro, A. Abbaspourrad, D. A. Weitz and S. T. Phillips, *Macromolecules*, 2013, **46**, 3309–3313.
233 A. Abbaspourrad, S. S. Datta and D. A. Weitz, *Langmuir*, 2013, **29**, 12697–12702.
234 W. J. Duncanson, L. R. Arriaga, W. L. Ung, J. A. Kopechek, T. M. Porter and D. A. Weitz, *Langmuir*, 2014, **30**, 13765–13770.
235 Y. H. Choi, J.-S. Hwang, S. H. Han, C.-S. Lee, S.-J. Jeon and S.-H. Kim, *Adv. Funct. Mater.*, 2021, **31**, 2100782.
236 G. Kaufman, K. A. Montejo, A. Michaut, P. W. Majewski and C. O. Osuji, *ACS Appl. Mater. Interfaces*, 2017, **9**, 44192–44198.
237 F. Huang, W.-C. Liao, Y. S. Sohn, R. Nechushtai, C.-H. Lu and I. Willner, *J. Am. Chem. Soc.*, 2016, **138**, 8936–8945.
238 S.-H. Jung, S. Bulut, L. P. B. Busca Guerzoni, D. Günther, S. Braun, L. De Laporte and A. Pich, *J. Colloid Interface Sci.*, 2022, **617**, 409–421.
239 R. Wang, K. Guo, W. Zhang, Y. He, K. Yang, Q. Chen, L. Yang, Z. Di, J. Qiu, P. Lei, Y. Gu, Z. Luo, X. Xu, Z. Xu, X. Feng, S. Li, Z. Yu and H. Xu, *Adv. Funct. Mater.*, 2022, **32**, 2113034.
240 S. A. Ryu, Y.-H. Hwang, H. Oh, K. Jeon, J. H. Lee, J. Yoon, J. B. Lee and H. Lee, *ACS Appl. Mater. Interfaces*, 2021, **13**, 36380–36387.
241 W. M. Hamonangan, S. Lee, Y. H. Choi, W. Li, M. Tai and S.-H. Kim, *ACS Appl. Mater. Interfaces*, 2022, **14**, 18159–18169.
242 S. Cho, J.-H. Kim, K. S. Yang and M. Chang, *Chem. Eng. J.*, 2021, **425**, 130645.
243 G. Tiwari, R. Tiwari, S. Bannerjee, L. Bhati, S. Pandey, P. Pandey and B. Sriwastawa, *Int. J. Pharm. Invest.*, 2012, **2**, 2.
244 T. Y. Lee, M. Ku, B. Kim, S. Lee, J. Yang and S.-H. Kim, *Small*, 2017, **13**, 1700646.
245 B. Liu, Y. Wang, F. Yang, X. Wang, H. Shen, H. Cui and D. Wu, *Colloids Surf., B*, 2016, **144**, 38–45.
246 M. Windbergs, Y. Zhao, J. Heyman and D. A. Weitz, *J. Am. Chem. Soc.*, 2013, **135**, 7933–7937.
247 C. E. Miles, C. Gwin, K. A. V. Zubris, A. J. Gormley and J. Kohn, *ACS Biomater. Sci. Eng.*, 2021, **7**, 2580–2591.
248 S.-H. Kim, J. W. Kim, D.-H. Kim, S.-H. Han and D. A. Weitz, *Small*, 2013, **9**, 124–131.
249 Y. H. Choi, S. Jeon and S. Kim, *Adv. Mater. Interfaces*, 2021, **8**, 2100538.
250 Y. Hu and J. Pérez-Mercader, *ACS Appl. Mater. Interfaces*, 2019, **11**, 41640–41648.
251 L. Jeon, Y. Kim, J. Yoon, H. Seo and H. Lee, *Small Struct.*, 2023, **4**, 2300200.
252 B. Kim, H. S. Lee, J. Kim and S.-H. Kim, *Chem. Commun.*, 2013, **49**, 1865–1867.
253 J. Oh, B. Kim, S. Lee, S.-H. Kim and M. Seo, *Chem. Mater.*, 2018, **30**, 273–279.
254 J. Wei, X.-J. Ju, R. Xie, C.-L. Mou, X. Lin and L.-Y. Chu, *J. Colloid Interface Sci.*, 2011, **357**, 101–108.
255 S. Wen, X.-J. Ju, W.-Y. Liu, Y.-Q. Liu, X.-Q. Pu, Z. Liu, W. Wang, R. Xie, Y. Faraj and L.-Y. Chu, *Engineering*, 2023, **24**, 114–125.
256 J. G. Werner, B. T. Deveney, S. Nawar and D. A. Weitz, *Adv. Funct. Mater.*, 2018, **28**, 1803385.
257 J. G. Werner, S. Nawar, A. A. Solovev and D. A. Weitz, *Macromolecules*, 2018, **51**, 5798–5805.
258 C. Owh, V. Ow, Q. Lin, J. H. M. Wong, D. Ho, X. J. Loh and K. Xue, *Biomater. Adv.*, 2022, **141**, 213100.
259 X.-X. Fan, R. Xie, Q. Zhao, X.-Y. Li, X.-J. Ju, W. Wang, Z. Liu and L.-Y. Chu, *J. Membr. Sci.*, 2018, **555**, 20–29.
260 H. Liu, J. Zhu, L. Hao, Y. Jiang, B. van der Bruggen, A. Sotto, C. Gao and J. Shen, *J. Membr. Sci.*, 2019, **587**, 117163.
261 X. Wang, D. Zhang, G. Wang, S. Wang, M. Si, J. Zhou, Y. Xu, G. Du, S. Yu Zheng and J. Yang, *Chem. Eng. J.*, 2023, **472**, 145185.
262 J.-W. Kim, S. S. Lee, J. Park, M. Ku, J. Yang and S.-H. Kim, *Small*, 2019, **15**, 1900434.
263 J.-W. Kim, S. H. Han, M. Ku, J. Yang and S.-H. Kim, *Chem. Mater.*, 2023, **35**, 4751–4760.
264 G. J. S. Dawes, L. E. Fratila-Apachitei, K. Mulia, I. Apachitei, G.-J. Witkamp and J. Duszczyk, *J. Mater. Sci.: Mater. Med.*, 2009, **20**, 1089–1094.
265 J. Wu, T. Kong, K. W. K. Yeung, H. C. Shum, K. M. C. Cheung, L. Wang and M. K. T. To, *Acta Biomater.*, 2013, **9**, 7410–7419.
266 S. Dash, P. N. Murthy, L. Nath and P. Chowdhury, *Acta Pol. Pharm.*, 2010, **67**, 217–223.

267 B. J. Crielaard, S. van der Wal, H. T. Le, A. T. L. Bode, T. Lammers, W. E. Hennink, R. M. Schiffelers, M. H. A. M. Fens and G. Storm, *Eur. J. Pharm. Sci.*, 2012, **45**, 429–435.
268 Z. Dong, Y. Ma, K. Hayat, C. Jia, S. Xia and X. Zhang, *J. Food Eng.*, 2011, **104**, 455–460.
269 Y. Yang, X. Li and S. Zhang, *RSC Adv.*, 2018, **8**, 29980–29987.